metals

Review

Addressing the Hydrogen Embrittlement Challenge in Future Hydrogen Pipelines: A Multiscale Review from Mechanisms to Material Design

Zongneng Zheng [1], Di Liu [1], Xinming Sun [1], Yinghu Wang [2], Yanhui Zhao [3,*] and Jianyan Xu [3]

[1] School of Petroleum Engineering, Karamay Vocational & Technical College, Karamay 834000, China
[2] National Center for Materials Service Safety, University of Science and Technology Beijing, Beijing 100083, China
[3] Sino-German Institute of Engineering, Shanghai Technical Institute of Electronics & Information, Shanghai 201411, China; hiyanran@nuaa.edu.cn
* Correspondence: pbaip2002@126.com

Abstract

To mitigate fossil fuel dependency and facilitate the transition towards a green economy, utilization of hydrogen energy has emerged as a paramount objective. Nevertheless, during transportation, this goal introduces novel challenges pertaining to material integrity, notably hydrogen embrittlement. This review systematically examines contemporary research on hydrogen embrittlement in natural gas pipelines conveying hydrogen blends and elucidates the hydrogen sources, permeation pathways, and embrittlement mechanisms. By scrutinizing the intrinsic material attributes and operational environments, this study provides an in-depth analysis of the pivotal factors influencing the susceptibility of pipeline steel to hydrogen embrittlement, thereby furnishing a theoretical foundation for the enduring safety of hydrogen pipelines.

Keywords: hydrogen embrittlement; pipeline steel; hydrogen transport; microstructure

1. Introduction

As global climate warming looms and a sweeping overhaul of the energy paradigm becomes inevitable, China has responded proactively by implementing a series of strategic plans aimed at catalyzing the growth and development of the renewable energy sectors [1]. The plan indicates that the utilization of clean energy sources, such as solar, wind, and hydrogen energy, will be a key task in the next phase, specifically emphasizing the need to vigorously develop low-cost production, transportation, and storage of hydrogen [2]. Hydrogen energy, especially 'green hydrogen' derived from renewable energy, is increasingly prominent in its strategic position owing to its multiple attributes, including zero carbon emissions, energy storage medium, and high-efficiency reducing agent.

However, owing to the prevailing constraints in infrastructure and a constellation of other influential factors, the financial outlay required for hydrogen conveyance and storage remains excessively burdensome [3]. Pipelines provide an economical and effective method for transporting hydrogen, and utilizing the existing natural gas pipeline network can significantly reduce hydrogen transport costs [4]. Many countries, including China, have established large-scale natural gas transmission pipelines. Transporting hydrogen mixed with natural gas through existing pipelines enables large-scale hydrogen transport at a lower cost [5,6]. Compared with their developed counterparts in Europe and America,

Academic Editor: Jin-Yoo Suh

Received: 4 February 2026
Revised: 29 March 2026
Accepted: 30 March 2026
Published: 17 April 2026

China's hydrogen pipeline infrastructure remains in its nascent stages of development, necessitating the resolution of a spectrum of pivotal challenges stemming from hydrogen blending practices. As shown in Table 1, the physicochemical properties of the natural gas changed after hydrogen blending. Therefore, the addition of hydrogen introduces new requirements for pipeline safety, compatibility of pipeline transportation equipment, and pipeline integrity. At Table 1, M is the molar mass.

Table 1. Physical Property Parameters Comparison Table of Methane and Hydrogen.

Physical Parameters	CH_4	H_2
M (g/mol)	16.04	2.01
Relative density	0.59	0.069
Critical temperature (K)	190.65	33.2
ρ (kg/m^3)	0.68	0.085

When hydrogen atoms are adsorbed onto the surface of a pipeline, they can infiltrate the material, driven by a concentration gradient. These atoms initially traverse the interstitial voids within the crystal lattice and may subsequently become ensnared by lattice imperfections, including vacancies, dislocations, grain boundaries, and nonmetallic inclusions. This process leads to the local accumulation of hydrogen atoms in the material substrate. Once the critical hydrogen concentration threshold is exceeded, this accumulation can cause crack initiation, eventually leading to brittle fracture, a phenomenon collectively known as hydrogen embrittlement (HE) [7], which adversely affects pipeline properties, such as fracture toughness and fatigue resistance [8,9], potentially culminating in catastrophic failure [10–12]. Alvaro et al. [13] found that a hydrogen environment reduces the ductility and fracture toughness of X70 pipeline steel. Zhang et al. [14] showed that X80 pipeline steel exhibits an increased fatigue crack growth rate and decreased fatigue life in a hydrogen environment. Evidently, pipeline failures caused by hydrogen embrittlement are an urgent issue that must be addressed [15]. It is necessary to establish a mechanism for the hydrogen embrittlement behavior of transmission pipeline steels, clarify the performance changes after hydrogen embrittlement occurs, ensure reliable and secure operation of gas transmission networks, and provide a reference basis for seeking effective anti-hydrogen embrittlement methods.

To provide a reference for relevant personnel, the author summarizes the sources and permeation process of hydrogen in natural gas–hydrogen-blended transmission pipeline steel, as well as the mechanisms of hydrogen embrittlement. A comprehensive discourse is presented on the determinants influencing the hydrogen embrittlement susceptibility of pipeline steel, examined through the dual lenses of inherent material properties and the operational service environment. An overview of the ramifications of hydrogen embrittlement in pipeline steel materials is provided, accompanied by an exposition of mitigation strategies aimed at curbing hydrogen embrittlement-induced damage. Finally, the application of approaches such as molecular dynamics and machine learning in hydrogen embrittlement research is briefly described. An evaluation framework is established, linking the mechanisms of hydrogen embrittlement to material quality and service environment, combined with computational predictions, with the aim of providing a theoretical basis and technical support to ensure the security of natural gas–hydrogen-blended transmission pipelines and energy transportation.

2. Hydrogen Sources and Permeation Processes in Hydrogen-Blend Transmission Pipeline Steel

Molecular hydrogen (H_2) cannot permeate metallic structures in its intact diatomic state; instead, it must dissociate into its atomic form (H) to facilitate its ingress into metals. The

https://doi.org/10.3390/met16040433

origin of hydrogen in materials can be systematically categorized into two primary types: internally sourced and externally introduced. For hydrogen-blended natural gas pipelines, internal hydrogen originates from smelting (hydrogen in the water vapor inside the furnace enters the molten pool and forms slag), welding (local smelting causes water in the welding rod to decompose), pickling (hydrogen generated by the reaction of part of the surface metal with acid entering the metal), and electroplating (hydrogen evolution process), among others. External hydrogen originates from the dissociative adsorption of H_2 in the hydrogen gas stream and cathodic hydrogen evolution reaction under pipeline operating conditions (impurities in natural gas, such as H_2S, CO_2, and H_2O, form accumulated liquid in pits on the interior surface of the pipeline, and wet H_2S and CO_2 induce electrochemical corrosion on the pipeline interior surface, generating hydrogen through the cathodic hydrogen evolution reaction) [16]. In a moist soil environment, electrochemical corrosion occurs on the outer wall of a pipeline, generating hydrogen through cathodic hydrogen evolution reactions. Soil microorganisms (such as sulfate-reducing bacteria, SRB) can also produce hydrogen as a byproduct of their metabolism (such as H_2S) through a 'poisoning' effect [17].

The sources of hydrogen in natural gas-blended hydrogen transmission pipeline steel, as well as its adsorption, dissolution, and diffusion, are illustrated in Figure 1. First, H_2 collected and transported inside the pipeline undergoes random Brownian motion and is physically adsorbed on the impacted inner surface of the pipeline through van der Waals forces. The hydrogen on the inner surface of the pipeline undergoes dissociation or is chemically adsorbed via cathodic hydrogen evolution caused by the electrochemical corrosion of the pipeline. The adsorbed hydrogen then dissolves into the subsurface, part of which combines with hydrogen gas and leaves the metal, while the other part diffuses through the metal lattice, vacancies, grain boundaries, dislocations, etc., and accumulates near areas of internal stress concentration or defects [18]. When the concentration of hydrogen accumulated at hydrogen traps exceeds the threshold concentration, hydrogen embrittlement is likely to occur. Under applied stress or even without external stress, pipeline steel may undergo hydrogen-induced cracking (HIC), leading to pipeline failure [19].

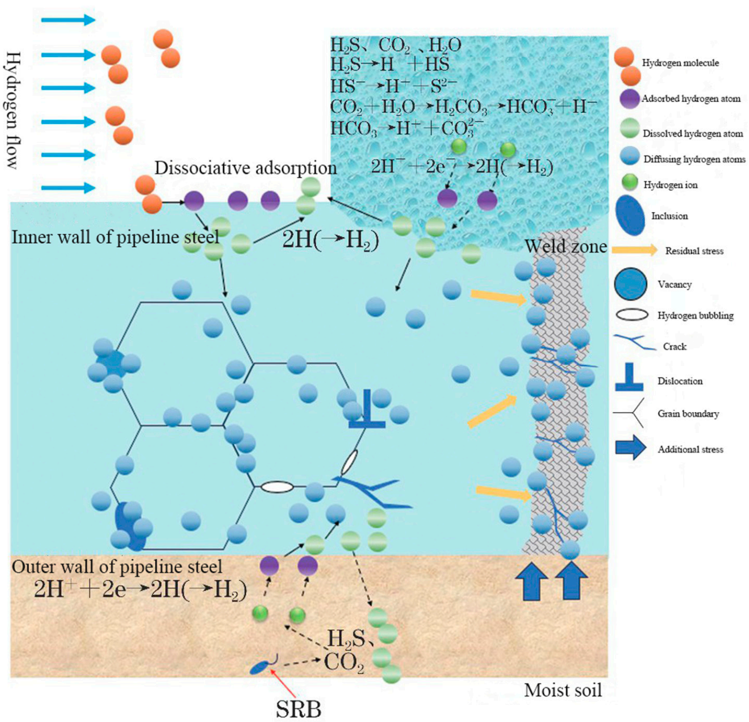

Figure 1. Schematic of source, adsorption, dissolution, and diffusion of H in hydrogen-blended transportation pipeline steel, adapted from ref. [18].

3. Research Progress on Hydrogen Embrittlement Mechanisms

In 1875, Johnson et al. [20] first discovered that the fracture stress of an iron wire significantly decreased after soaking in acid for a few minutes. Further research has found that hydrogen causes embrittlement only when it exists in the atomic form, marking the first report of hydrogen embrittlement. Hydrogen embrittlement is a phenomenon in which metallic properties are severely degraded owing to hydrogen adsorption during smelting, processing, and service. Hydrogen embrittlement typically occurs without warning, and fractures occur suddenly. In recent decades, hydrogen-induced failures have been reported in fields such as bridge construction, petrochemicals, and aerospace [21–23]. A notable example is the hydrogen-induced fracture of bolts on the San Francisco-Oakland Bay Bridge [23]. Hydrogen embrittlement incidents pose a significant risk to the safety and reliability of materials in service.

The sources of hydrogen atoms in metals are complex and diverse. During smelting and casting, the use of hydrogen-containing raw materials (such as damp charges) can lead to the dissolution of hydrogen atoms in the metal. Subsequent processing stages (such as electroplating and pickling) can also introduce hydrogen atoms [24]. When metals are in service in humid air, hydrogen atoms can enter the metal through adsorption and diffusion. Under stress corrosion conditions, the synergistic effects of mechanical stress and chemical corrosion can significantly accelerate hydrogen adsorption.

The distribution of hydrogen atoms within metallic structures is closely related to microscopic structural defects. In an ideal lattice, hydrogen atoms tend to dissolve in interstitial positions, forming an interstitial solid solution. However, real metals usually have crystal defects, such as microcracks, phase boundaries, grain boundaries, dislocations, vacancies, and precipitates. These sites exhibited higher lattice distortions, creating stress fields. The stress fields at the defect sites have a high affinity for hydrogen atoms, making it easy to trap hydrogen atoms. The sites that readily trap hydrogen atoms are commonly referred to as hydrogen traps, as shown in Figure 2.

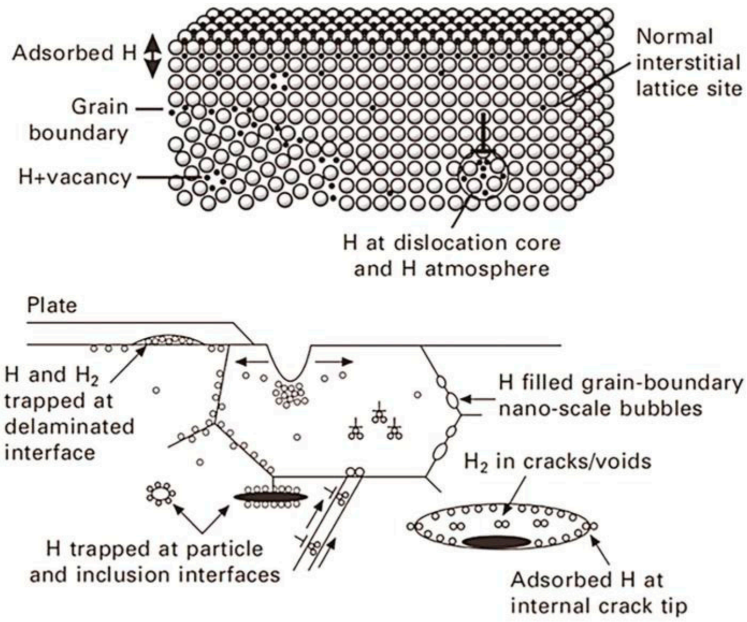

Figure 2. Schematic diagram of common hydrogen traps in steel, reprinted with permission from ref. [25].

Following decades of intensive scholarly investigation, more than a dozen hydrogen embrittlement mechanisms have been formulated to elucidate the intricate phenomenon of hydrogen-induced degradation across diverse metallic substrates. The activation and impact of specific hydrogen embrittlement mechanisms are closely related to the hydrogen concentration, crystal structure, and microstructure of the alloy [26,27]. Each hydrogen embrittlement mechanism has its own characteristics, as detailed below.

(1) Hydrogen enhanced decohesion (HEDE)

The hydrogen-induced reduction in atomic bonding strength theory is also known as the Weak Bond Theory. The core idea is that hydrogen reduces the cohesive strength of the metal lattices and grain boundaries, thereby lowering the stress threshold for cracking in hydrogen-enriched regions [28–30]. In 1926, Pfeil et al. [31] first mentioned that hydrogen atoms could reduce interatomic binding forces. Troiano et al. [29] further pointed out that the 1 s electron of the hydrogen atom can access the vacant d-orbitals of transition metals, resulting in increased interatomic repulsions. Later, Oriani et al. [30] conducted quantitative studies on the HEDE mechanism and found that the more serious the hydrogen concentration, the weaker the interatomic bonding in the metals. When hydrogen concentration exceeds a particular value, hydrogen-induced cracking can occur even under conditions far below the tensile strength. Figure 3 states the HEDE mechanism: during deformation, hydrogen tends to accumulate at crack tips and grain boundaries. This decreases the interatomic bonding at the crack tip and promotes crack propagation. Furthermore, hydrogen atoms enriched at the phase and grain boundaries also reduce interatomic bonding at the interface, leading to possible grain boundary cracking under lower stress conditions. Before grain boundary cracking occurs, large-scale dislocation slip does not occur, making the intergranular fracture features on hydrogen-induced brittle fracture surfaces, where the HEDE mechanism is dominant, evident. However, the HEDE mechanism has several limitations. Most reports on hydrogen-reducing atomic bonding strength are based on first-principles calculations, and there is still a lack of direct experimental evidence [32]. Furthermore, the HEDE mechanism alone cannot fully explain the plastic features of the crystal planes in the case of intergranular fractures, such as slip bands or tear ridges.

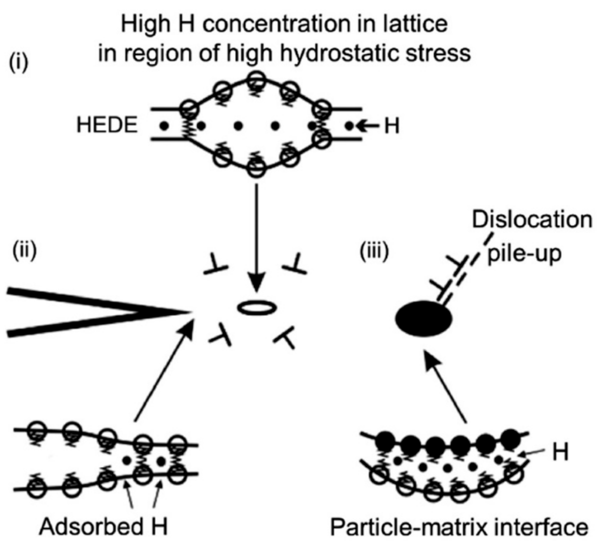

Figure 3. Schematic diagram of hydrogen reducing atomic bond strength theory, reprinted with permission from ref. [25].

(2) Hydrogen-enhanced localized plasticity theory (HELP)

The hydrogen enhanced localized plasticity (HELP) theory posits that hydrogen diminishes the resistance to dislocation migration, thereby fostering accelerated dislocation motion at the crack tips and consequently facilitating the propagation of cracks [33,34], as visually demonstrated in Figure 4. In addition, local hydrogen enrichment can promote

https://doi.org/10.3390/met16040433

dislocation motion in this area, causing localized plastic deformation at lower stress levels and leading to premature crack nucleation. Ferreira et al. [35] verified the HELP mechanism through in situ TEM experiments, observing that hydrogen can promote dislocation movement while reducing the distance between dislocations. Zhao et al. [36] used molecular dynamics simulations of nanoindentation to elucidate the effects of hydrogen on dislocation slip resistance, further confirming that hydrogen can lower crucial stress for dislocation nucleation. Moreover, Tabata et al. [37] showed that in materials with higher hydrogen concentrations, the dislocation motion rate is faster, indicating that hydrogen can increase the rate of dislocation movement. These experimental results effectively support the HELP mechanism proposed in this study.

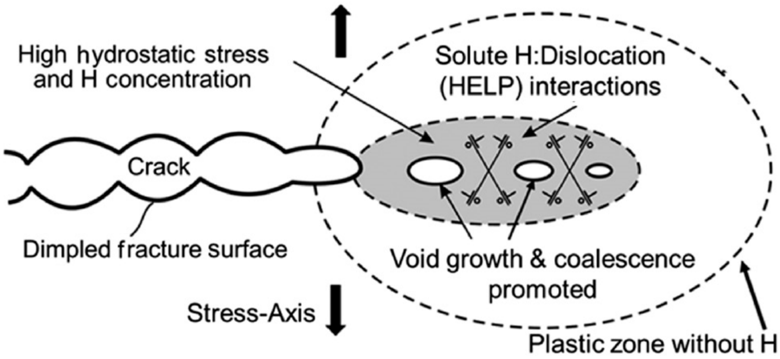

Figure 4. Schematic diagram of hydrogen-promoted local plastic deformation theory, reprinted with permission from ref. [25].

Hydrogen-induced cracking dominated by the HELP mechanism is usually accompanied by local plastic deformation and dislocation slip; therefore, some features such as dimples and tear ridges can be observed on the fractured face. It is widely believed that the essence of the HELP mechanism involves hydrogen reducing the critical resolved shear stress necessary for dislocation movement and promoting the multiplication and motion of dislocations, thereby intensifying the local plastic deformation.

(3) Hydrogen enhanced strain induced vacancy formation theory (HESIV)

The proposed mechanism indicates that hydrogen can reduce the vacancy formation energy in materials, thereby increasing the density of vacancies [38,39]. The aggregation of vacancies, in turn, easily forms micropores, increasing the susceptibility to hydrogen-induced cracking. Kirchheim et al. described the process by which hydrogen reduces the vacancy formation energy from a thermodynamic perspective as Equation (1):

$$E_V^H = E_V^0 - n\mu_H \quad (1)$$

In the above formula, E_V^0 is the vacancy formation energy without hydrogen, n is the number of hydrogen atoms in the vacancy, and μ_H is the chemical potential of the hydrogen atoms. As the hydrogen concentration increased, the vacancy formation energy decreased.

Saitok et al. [40] confirmed the HESIV mechanism hypothesis using TDS and positron annihilation experiments. Their experimental results showed that samples with higher hydrogen content had longer electron annihilation lifetimes and higher vacancy concentrations. However, the HESIV mechanism has certain limitations. Generally, the formation of holes from vacancy clusters requires a significant driving force and very high hydrogen concentration to generate a large number of hydrogen-induced micropores. However, hydrogen-induced fractures can occur in metals at extremely low hydrogen concentrations. Therefore, the HESIV mechanism has not yet been fully developed and requires further investigation.

(4) Hydrogen pressure theory

In metallic materials, hydrogen can be adsorbed at defects such as phase boundaries, grain boundaries, dislocations, and microvoids. These defect locations have relatively large free volumes and elastic strain fields, which can trap hydrogen atoms [41,42]. Hydrogen atoms accumulate at these defect sites, combine to form hydrogen molecules, and generate hydrogen pressure. According to Kirchheim [43], the local hydrogen pressure (P) is related to the hydrogen concentration at defects by the following Equation (2):

$$C_H = Ae^{(-\frac{\Delta H}{RT})}\sqrt{P} \quad (2)$$

In the above equation, A and R are constants, ΔH is the heat of dissolution, and T is the absolute temperature. According to this formula, hydrogen pressure is proportional to the square of the hydrogen concentration. Defect sites in the crystal easily adsorb hydrogen atoms, which can then combine to form hydrogen molecules, leading to a locally higher hydrogen pressure. Simultaneously, this locally higher hydrogen pressure causes an increase in the local stress in that region, which in turn induces further accumulation of hydrogen atoms at the defects. Upon surpassing the critical hydrogen pressure threshold that the material can endure, it undergoes plastic deformation, as dictated by the interplay between the mechanical stress and hydrogen-induced effects.

4. Factors Affecting HE Behavior of Pipeline Steel

4.1. Hydrogen Embrittlement Behavior of X-Series Hydrogen-Added Pipeline Steel

In Europe, hydrogen pipelines typically operate under transmission pressures within the range of 2–10 MPa, predominantly utilizing seamless steel pipes with diameters spanning from 0.3 to 1.0 m. Pipe materials predominantly comprise low-strength pipeline steels, such as X42, X52, and X56. In contrast, hydrogen pipelines in the United States are predominantly laid underground, with transmission pressures generally not exceeding 7 MPa. The materials employed in this study mainly consisted of pipeline steels ranging from X52 to X80, with an anticipated service life of 15–30 years. On a global scale, numerous scholars have investigated the compatibility of pipeline steels with high-pressure hydrogen environments. For instance, Wei [44] conducted fracture toughness of X80 steels drops in a logarithmic or power-law trend with rising H_2 pressure. Similarly, Briottet [45] systematically performed a battery of tests on X80 pipeline steel in a high-pressure hydrogen environment, including slow-strain-rate tensile, fracture toughness, disk, fatigue crack growth, and WOL tests. The results revealed that, although the elastic modulus, yield strength, and tensile strength of the material remained relatively unchanged in a hydrogen environment, its plasticity and fracture toughness were significantly diminished, and the fatigue crack growth rate was markedly accelerated. Furthermore, Hardie [46] investigated the sensitivity of X60, X80, and X100 pipeline steels through electrochemical hydrogen charging. Their findings indicated that when the hydrogen charging current density reached a certain threshold, the sensitivity to hydrogen embrittlement increased substantially with increasing material strength. The hydrogen embrittlement behavior of pipeline steels in the X42–X100 series is summarized in Table 2. The hydrogen embrittlement index of pipeline steel is affected by multiple factors, resulting in varying degrees of resistance to hydrogen embrittlement.

In conclusion, it is imperative to ascertain, through experimental means, how the interplay of various factors with the strain rate impacts the hydrogen embrittlement sensitivity of pipeline materials.

Table 2. Comparison of Hydrogen Embrittlement Behavior of X Series Hydrogen-Added Pipeline Steels (note: some original references did not report pressure, and only available data are presented), adapted from ref. [47–52].

Brand	Strain Rate/s^{-1}	Experimental Environment	Current Rate/(mA × cm^{-2})	Hydrogen Embrittlement Index/%
X42 [47]	5.4×10^{-5}	H_2SO_4	0.5, 1, 2.5	34, 42, 59
X52 [48]	5.37×10^{-5}	H_2SO_4	10, 20	72, 75
X70 [49,50]	3.75×10^{-5}	Pure H_2 (1.2 MPa)		22~25
	2.62×10^{-5}	H_2-CH_4 (0.1 MPa)		3, 83
X80 [51,52]	5×10^{-5}	Pure H_2		0, 41, 67, 68
	1×10^{-5}	H_2SO_4	1	63
X100	2×10^{-5}	H_2SO_4	25	46.3

4.2. Intrinsic Factors of Pipeline Steel Material

4.2.1. Alloy Composition

Elements such as sulfur, phosphorus, aluminum, manganese, and silicon tend to form segregations or inclusions during steelmaking or rolling, which can increase the susceptibility to hydrogen embrittlement. Alloying elements that form nanoscale carbides with carbon can provide irreversible traps with high binding energies (traps from which hydrogen cannot easily escape) and can also increase the number of reversible traps (traps from which hydrogen can escape) by refining the grain size, making the distribution of hydrogen in steel more uniform, and inhibiting its accumulation at defect sites, thereby enhancing the resistance to hydrogen embrittlement. Table 3 presents the differences in the hydrogen embrittlement sensitivity and mechanical properties of various steels.

Table 3. Effects of different alloying elements on the mechanical properties and hydrogen embrittlement susceptibility of steels, adapted from ref. [53–61].

Steel Grade	Alloy Element	Number of Hydrogen Traps	Hydrogen Diffusion Coefficient	Precipitation Strengthening
Martensitic steel [53]	Cr	Increase	Decrease	Increase
Austenitic steel [54]	Cu		Decrease	
High-strength steel [55]	Mo	Increase		Increase
X70 steel [56]	Mn		Increase	
Low carbon steel [57]	Nb	Increase	Decrease	Increase
High-strength steel [58–60]	Ti	Increase		
Ferritic steel [61]	V	Increase		

Shi et al. [62] found that nanoscale copper-rich phases (copper mass fractions of 1.06%, 1.46%, and 2.00%) can promote the formation of hydrogen traps, distribute hydrogen evenly, and avoid local hydrogen embrittlement. Yoo et al. [63] also indicated that the addition of copper (at mass fractions of 1% and 3%) decreased the hydrogen diffusion rate and effectively enhanced the resistance of the material to hydrogen embrittlement. The incorporation of vanadium results in the formation of efficient hydrogen-trapping sites within the material substrate, thereby reducing the quantity of diffusible hydrogen and consequently diminishing the propensity for hydrogen embrittlement. As the vanadium content increased, the precipitation of vanadium carbide nanoparticles within the steel increased, resulting in an increased number of effective hydrogen traps and a marked decline in the hydrogen diffusion coefficient. Notably, steel fortified with 0.13% vanadium demonstrated the highest resistance to hydrogen embrittlement, as evidenced by experimental findings [64]. Furthermore, corroborative studies conducted by Yang et al. [65] and Dong et al. [66] revealed that the addition of vanadium enhances the hydrogen embrittlement resistance of steel, underscoring the robustness of this alloying strategy.

Molybdenum, a strong carbide-forming element, effectively reduces the susceptibility of materials to hydrogen embrittlement. In Cr-Mo steel, Mo mitigates the segregation of impurities, such as sulfur and P, at the grain boundaries, thereby enhancing the steel's resistance to hydrogen embrittlement. Fu et al. [67] and Zhang et al. [68] found that doping chromium-molybdenum steel with molybdenum makes it easier to dissolve hydrogen in iron crystals because molybdenum increases the activation energy of hydrogen diffusion and significantly reduces its diffusion coefficient. Simultaneously, molybdenum mainly exists in the form of solute atoms and is polarized at the grain boundaries. The presence of a large number of molybdenum atoms in the substrate can delay the diffusion of hydrogen to the inclusions, thereby delaying the onset of cracks [69]. For 42CrMo steel and AISI4130 chromium-molybdenum steel, the ideal mass fraction of Mo is 1.15% and 0.75–0.90%, respectively, while the mass fraction of Mo in chromium-molybdenum steels commonly used in pressure vessels (e.g., 30CrMo, 4130X, and 34CrMo4 steels) [70] should be 0.25–0.30%.

The niobium in steel can not only refine grains and increase strength, but nanosized carbides formed with carbon can also hinder the diffusion of hydrogen. Zhang et al. [71] found that nanosized niobium carbides formed after adding niobium can delay the formation of hydrogen blisters. The addition of niobium can also reduce the proportion of $\Sigma 3$/large-angle grain boundaries, thereby increasing the resistance to crack propagation, while the precipitation of NbC hinders hydrogen-dislocation interactions, reducing local plastic deformation [72]. However, carbide inclusions larger than 5 μm in steel can become centers for hydrogen accumulation and initiation points for hydrogen-induced cracking, which is unfavorable for improving the resistance of steel to hydrogen-induced cracking [73]. Therefore, the size of the alloy carbides should be controlled during heat treatment. While alloy composition provides the chemical foundation, its effect on HE susceptibility is ultimately manifested through the microstructures that develop during processing, which we discuss in the following section.

4.2.2. Microstructure of Pipeline Steel Materials

Generally, in common pipeline steel microstructures, the susceptibility to hydrogen embrittlement is often reported to follow a trend where martensite exhibits higher susceptibility than bainite and ferrite, while austenite shows the lowest susceptibility due to its high hydrogen solubility and low diffusivity [74]. However, this ranking is highly dependent on specific testing conditions, such as hydrogen charging method, stress state, strain rate, and the detailed morphological characteristics of each phase [75,76]. Simultaneously, it was observed that the hydrogen diffusion coefficient exhibited inverse proportionality with respect to the martensite content within the material. The susceptibility of bainite to hydrogen embrittlement is predominantly governed by its morphological characteristics and spatial distribution [77]. This phenomenon can be attributed to the fact that grain boundaries and dislocations substantially augment the specific surface area, thereby offering an increased number of adsorption sites for hydrogen atoms to reside in [78,79].

4.2.3. Precipitate Phase

As service environments become increasingly harsh, precipitates play an important role in enhancing the strength of hydrogen pipeline steels. The development trend is toward nano structuring, composite formation, and deepening interface control, thereby offering a pathway to develop high-strength hydrogen pipeline steels with improved HE resistance. It is crucial to note that the goal is not merely to increase strength, but rather to achieve a homogeneous distribution of nano-sized precipitates that act as effective hydrogen traps. Studies have reported that under specific experimental conditions, the hydrogen-trapping ability of single precipitates can follow a trend such as NbC > TiC > VC > Mo_2C [80]. However, this comparison is highly sensitive to precipitate size, coherency, testing conditions, and should not be taken as absolute. Taking Mo and Nb as an example, the hydrogen trapping capacity of (Mo, Nb) C composite precipitates formed by Nb and Mo is much higher than that of NbC [81,82]. Research has revealed that mobile dislocations possess the capability to "transport" hydrogen towards grain boundaries. This process results in a swift surge in hydrogen concentration at these boundaries, ultimately triggering and facilitating the initiation and propagation of cracks [83,84]. Consequently, inhibiting the hydrogen-mediated migratory behavior of dislocations has emerged as a highly effective approach to augmenting the resistance of hydrogen pipeline steels against hydrogen embrittlement. Illustratively, the incorporation of (V, Nb) C precipitates obstructs dislocation motion, thereby curbing hydrogen aggregation and, in turn, significantly enhancing the material's durability in the face of hydrogen embrittlement challenges [85].

At the same time, different precipitate structures have significantly different hydrogen-trapping capabilities. For example, the hydrogen trapping capacity of copper-rich precipitates with different structures decreases in the order 9R > FCC > B2 > BCC [86] (9R and B2 are precipitate structures). The hydrogen trapping capability of copper-rich precipitates with different structures is shown in Figure 5. In addition, the hydrogen-trapping ability of the precipitates is related to their dislocation pinning effect. When mobile dislocations are impeded by precipitates during movement, they behave similarly to Frank-Read sources; the dislocations bend and eventually form hydrogen-rich dislocation loops, which enhances the hydrogen trapping ability of the precipitates [87]. The activation energies of dislocations, grain boundaries, and coherent interface carbides are similar, suggesting that coherent interface carbides act as reversible hydrogen traps [88]. Currently, many studies indicate that precipitates can reduce hydrogen embrittlement susceptibility in hydrogen transportation pipeline steels; however, these conclusions are based on experiments and simulations and lack direct evidence of how hydrogen atoms interact with precipitates. Additionally, issues remain, such as unclear interaction relationships when different types of precipitates (coherent interfaces, semi-coherent interfaces, and incoherent interfaces) coexist and the difficulty in quantifying the synergistic effects of multi-scale interfaces. From a materials design perspective, this suggests that controlling precipitate dispersion is equally important as controlling precipitate composition. Furthermore, we identify a critical knowledge gap: the synergistic or competitive effects of multiple precipitate types and interfaces at different scales remain poorly understood. Addressing this gap through integrated experimental and modeling approaches represents a key priority for future research.

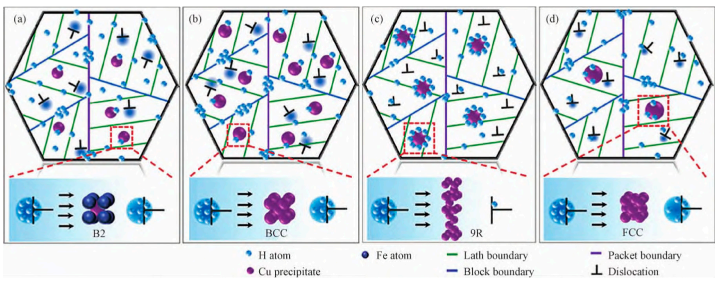

Figure 5. Schematics of hydrogen capture capacity of four copper-rich precipitates with different structure: (**a**) B2-Cu; (**b**) BCC-Cu; (**c**) 9R-Cu; (**d**) FCC-Cu. Reprinted with permission from ref. [86].

4.2.4. Inclusions and Segregation

Not only by its microstructural features, alloying constituents, and precipitate phases, but also by the presence of inclusions and segregation phenomena that arise throughout the processing stages result in hydrogen embrittlement of hydrogen transmission pipeline steel. Studies have shown that the number, size, and volume fraction of inclusions can affect the hydrogen embrittlement susceptibility [89,90]. MnS is a common inclusion in pipeline steel and is generally believed to increase hydrogen embrittlement susceptibility [91,92] because hydrogen atoms tend to accumulate mainly at the MnS-substrate interfaces. Nevertheless, the presence of micron-scale MnS inclusions facilitates a more homogenous dispersion of hydrogen atoms within the substrate, consequently enhancing the hydrogen embrittlement resistance of X70 pipeline steel [93]. In the pursuit of precisely tailoring the size and morphological attributes of MnS inclusions, Ti is routinely introduced to promote the generation of more complex TiN-MnS composite precipitates [94,95]. Jin et al. [96] research on X100 pipeline steel revealed that inclusions significantly influenced hydrogen embrittlement susceptibility, with cracks predominantly linked to Al- and Si-rich spherical inclusions.

It is generally believed that segregation can act as a "fast path" for hydrogen diffusion, accelerating hydrogen transport. Simultaneously, higher hydrogen concentrations at the segregation sites can trigger crack initiation. Nevertheless, research indicates that the segregation of specific elements can enhance the resistance of steel to hydrogen embrittlement. For instance, Mo segregation at prior austenite grain boundaries impedes crack propagation, whereas B, Mo, and W mitigate hydrogen atom accumulation at grain boundaries, thus reducing failure risks from excessive local hydrogen concentrations. This effect strengthens with an increased segregation concentration of alloying atoms [97]. Likewise, modulating the chemical heterogeneity of Mn in austenite has demonstrated enhanced hydrogen embrittlement resistance in high-strength steels [98]. This is mainly due to three reasons: (1) Mn-rich regions (Mn atomic fraction of 14–16%) increase the stability of austenite compared to Mn-poor regions (Mn atomic fraction of 11–12%), suppressing the transformation of austenite to α'-martensite, thus reducing hydrogen solubility and hydrogen diffusion coefficients. (2) Austenite blunts hydrogen-induced cracks, thereby slowing crack propagation. (3) The chemical heterogeneity of Mn obstructs crack initiation and propagation. As shown in Figure 6, Mn-rich regions can act as "ligaments" bridging cracks, further lowering the stress intensity at the crack tips and hindering crack growth, as evident from Figure 7b. This approach to controlling the chemical heterogeneity of Mn within austenite provides valuable guidance for enhancing the hydrogen embrittlement resistance of hydrogen transmission pipeline steel.

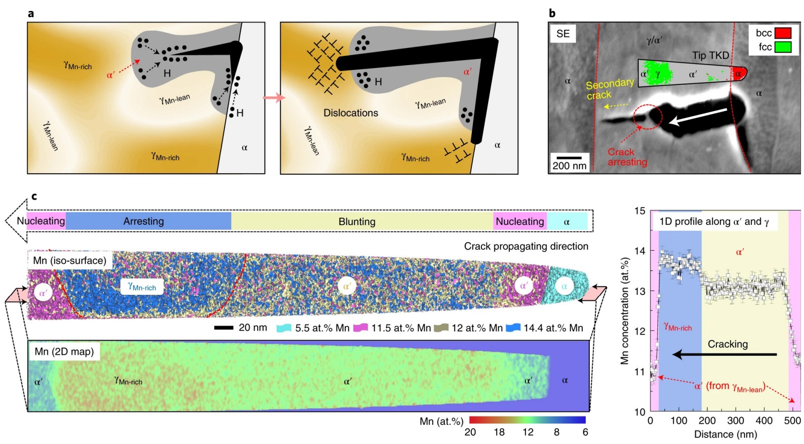

Figure 6. Chemical heterogeneity of Mn hindering crack initiation and growth: (**a**) schematic illustration showing the crack-arresting mechanisms, (**b**) a representative blunted and arrested H-induced crack in the H-charged and fractured chemical-heterogeneity-manipulated steel (total H amount 6.3 ppmw), and (**c**) the APT results for the tip shown in (**b**), reprinted from Ref. [98].

4.2.5. Grain Boundary

Hydrogen atom aggregation at grain boundaries reduces the interfacial binding energy, inducing hydrogen embrittlement. Grain boundaries exhibit dual effects: they can trap hydrogen to inhibit embrittlement, yet also serve as rapid diffusion pathways, enabling "short-circuit" hydrogen transport that exacerbates embrittlement. Studies have shown that the probability of hydrogen-induced cracks occurring at random grain boundaries is significantly higher than that at special grain boundaries [99]. Some special grain boundaries exhibit stronger hydrogen embrittlement resistance, such as Σ3, which has lower energy, so it has a lower hydrogen capture binding energy than other grain boundaries, resulting in less hydrogen polarization [100]. Consequently, enhancing the hydrogen embrittlement resistance of hydrogen pipeline steel is achievable by adjusting the grain boundary ratio, specifically by optimizing the characteristic distribution of grain boundaries and elevating the proportion of special grain boundaries. This approach embodies the core mechanism of grain boundary engineering in augmenting the resistance of materials to hydrogen embrittlement. For example, increasing the special grain boundary ratio of TWIP steel through grain boundary engineering effectively reduces the number of sites of crack initiation and hinders further crack propagation [101]. The incorporation of alloying elements, such as Cu, elevates the fractions of high-angle and special grain boundaries. Specifically, a higher proportion of high-angle grain boundaries enhances the hydrogen trap density and decelerates hydrogen diffusion, whereas an increased proportion of special grain boundaries effectively impedes crack propagation [102]. Figure 7 illustrates the propagation of hydrogen-induced cracks across various special grain boundaries, revealing a marked suppression of crack advancement in steels containing a high proportion of such boundaries, in contrast to those with a lower proportion. Although grain boundary engineering has yielded some advancements in enhancing the hydrogen embrittlement resistance of hydrogen pipeline steel, challenges persist, notably in the intricate design and regulation of grain boundaries. Future studies could integrate in situ characterization techniques to further elucidate the dynamic segregation mechanisms of hydrogen atoms across diverse grain boundary types, thereby guiding the development of a novel generation of high-strength, tough hydrogen pipeline steels. Grain boundaries are not the only lattice defects that influence hydrogen behavior; dislocations and vacancies, discussed next, also play critical roles in hydrogen trapping and transport.

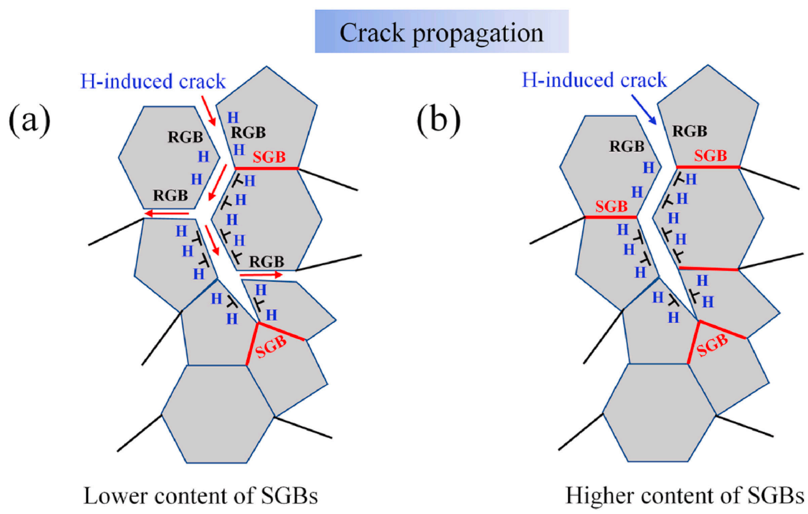

Figure 7. Hydrogen-induced crack propagation under different SGB ratios: (**a**) low content of SGB; (**b**) high content of SGB, reprinted from Ref. [102].

4.2.6. Dislocations and Vacancies

Vacancies can capture hydrogen and inhibit its diffusion, thereby significantly increasing the equilibrium concentration of vacancies [103]. However, the number of hydrogen atoms that a single vacancy can accommodate remains controversial. Nazarov et al. [104] found that a single vacancy in a face-centered cubic iron substrate is an efficient and spacious trap that can accommodate up to six hydrogen atoms. Cheng et al. [105] suggested that under vacuum conditions, a single vacancy can hold 3 hydrogen atoms. He et al. [106] discovered that vacancies in γ-Fe not only act as traps for capturing hydrogen but also reduce the activation energy for hydrogen diffusion, promoting hydrogen mobility. Dislocations can serve as reversible traps for hydrogen; when hydrogen enters the interior of a metal, it interacts with dislocations, affecting the transmission of hydrogen. Jemblie et al. [107] found that hydrogen at dislocations in hot-rolled composite steel pipes reduces their toughness, confirming the conclusion that hydrogen accumulation at dislocations increases the material's sensitivity to hydrogen embrittlement. During plastic deformation, screw dislocations in steel play a dominant role in its toughness, and hydrogen promotes screw dislocation movement, causing localized plasticity. However, excessive localized plasticity can lead to concentrated local deformation, forming microcracks and other defects, which in turn become sites for hydrogen accumulation and stress concentration, thereby increasing the susceptibility of the material to hydrogen embrittlement.

4.2.7. Other Factors

The hydrogen embrittlement susceptibility of hydrogen transport pipeline steel is governed not only by composition, microstructure, and precipitates, but also by residual stress, temperature, and hydrogen pressure. Residual stress primarily modulates embrittlement susceptibility by influencing hydrogen diffusion and accumulation as well as crack initiation and propagation [108]. Residual tensile stress accelerates hydrogen diffusion, fostering the initiation and propagation of hydrogen-induced cracks. Conversely, residual compressive stress generally enhances the resistance of pipeline steel to hydrogen embrittlement by acting as a specific form of static mean stress, diminishing the effective stress amplitude ($\Delta\sigma_e$) and intensity factor (ΔK_e) at the crack tip, thereby markedly decelerating crack propagation. During the service of hydrogen transport pipeline steel, the relaxation of residual stress may affect hydrogen distribution and diffusion, thus impacting the steel's hydrogen embrittlement sensitivity. Pure hydrogen pipeline transportation involves much higher pressures than hydrogen-mixed transportation, and increased hydrogen pressure leads to higher hydrogen embrittlement sensitivity as hydrogen solubility increases with the square root of hydrogen pressure. For example, the fatigue life of X80 pipeline steel decreases with increasing hydrogen pressure [109]. Nevertheless, the hydrogen embrittlement susceptibility of pipeline steel does not escalate continuously with increasing hydrogen pressure; instead, a threshold exists, beyond which further pressure increments do not significantly influence embrittlement sensitivity [110].

Temperature modulates the susceptibility of pipeline steel to hydrogen embrittlement through its impact on the hydrogen diffusion and accumulation dynamics. Temperature exerts a threshold-dependent effect on material hydrogen embrittlement susceptibility; embrittlement remains absent below this threshold, while exceeding it prevents the hydrogen concentration from attaining the critical level. Consequently, hydrogen embrittlement manifests solely within a specific temperature range [111,112]. For instance, the threshold temperatures for the peak hydrogen embrittlement susceptibility in X70 pipeline steel are 293 and 283 K under charging currents of 10 and 20 mA/cm^2, respectively [113]. In X80 pipeline steel, the hydrogen diffusion coefficient escalates with temperature within the 300–325 K range, with 315 K marking the threshold for maximal hydrogen embrittlement susceptibility [114]. Figure 8 illustrates the mechanical characteristics of X80 pipeline steel subjected to in situ hydrogen charging across varying temperatures.

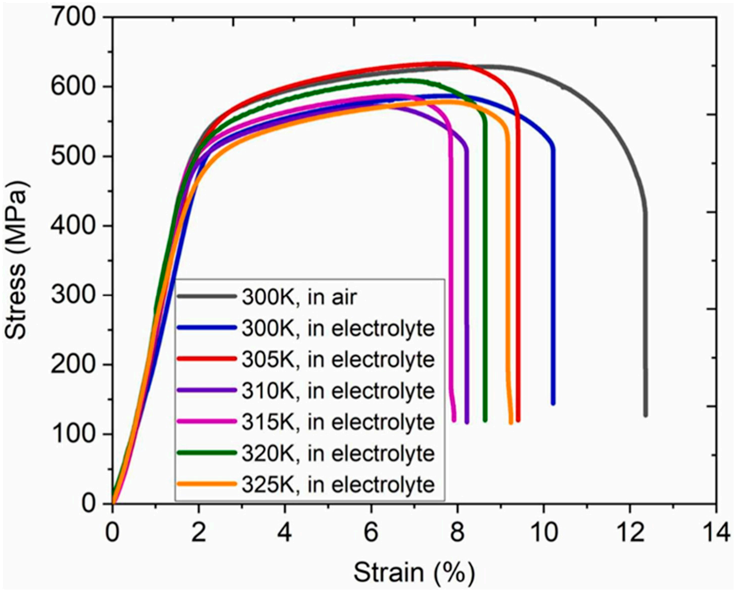

Figure 8. Mechanical properties of X80 pipeline steel at different temperatures filled with hydrogen in situ, reprinted with permission from ref. [114].

4.3. Service Environment

While the intrinsic material factors discussed in Section 4.2 determine the baseline HE susceptibility of a given pipeline steel, the actual in-service performance is profoundly influenced by the external environment to which the pipeline is exposed. These service factors including hydrogen concentration, temperature, stress state, and pressure interact with the material's microstructure to govern hydrogen uptake, diffusion, and accumulation.

4.3.1. Hydrogen Concentration

The density difference between hydrogen and natural gas in hydrogen-blended pipelines easily leads to an uneven hydrogen concentration distribution [115]. A critical aspect of hydrogen concentration distribution is gas stratification. Due to the significant density difference between hydrogen (0.085 kg/m^3) and methane (0.68 kg/m^3), gravity can induce stratification under low-flow or stagnant conditions. This can lead to local hydrogen concentration may be substantially higher than the average blending ratio, in extreme cases potentially approaching 100%. And local high hydrogen concentrations can increase the susceptibility of steel pipes to hydrogen embrittlement and reduce mechanical performance [116]. If the natural gas transport system with hydrogen blending is controlled under lower pressure (less than 5 MPa) and higher flow velocity (greater than 10 m·s^{-1}), the gas mixing uniformity improves, the probability of hydrogen atoms diffusing into the metal decreases, and the risk of hydrogen embrittlement is relatively reduced [115]. With increasing hydrogen concentration, the plasticity of X52 steel markedly declines, while its hydrogen embrittlement index surges [48]. Similarly, the plasticity and fracture toughness of X70 and X80 steels diminish significantly, accompanied by a pronounced rise in the fatigue crack growth rate [117,118]. Conversely, the yield and tensile strengths of the X100 steel decreased [119]. Notably, a critical hydrogen concentration threshold exists in the relationship between the hydrogen embrittlement index and hydrogen concentration for X70 steel. Below this threshold, the index initially increased rapidly before rising gradually with further hydrogen concentration increments. Above this threshold, hydrogen blisters emerge on the X70 steel surface, and internal hydrogen-induced cracks develop [120].

4.3.2. Temperature

Temperature variations influence the diffusion and aggregation of hydrogen atoms, thereby modulating the hydrogen embrittlement (HE) behavior of steel [121]. Currently, research on the temperature effects on HE in pipeline steel in gaseous environments is scarce, although studies on other steels in liquid settings offer valuable insights. Earlier investigations, Doshida et al. [122] similarly reported that HE susceptibility in steel increases with temperature above −30 °C. However, the effect of temperature on the HE remains contentious. Recent studies by Xing et al. [123] on X90 steel, conducted via slow strain rate tensile tests in simulated formation solutions and air, identified a temperature threshold for HE susceptibility that does not vary monotonically with temperature. The peak HE susceptibility for the X90 steel occurred at 313 K, increasing below this threshold and decreasing above it. Momotani et al. [124] investigated the temperature-dependent HE susceptibility of low-carbon martensitic steel from −100 to 100 °C, finding that within 0–100 °C, tensile strength and elongation decrease with falling temperature, but rise again below 0 °C, suggesting maximum HE susceptibility at room temperature. These findings underscore the significant impact of temperature on HE behavior. Thermodynamically, low temperatures impede hydrogen atom penetration and diffusion, hindering aggregation, whereas high temperatures enhance the activation energy and diffusion rates, reducing hydrogen accumulation at dislocations and grain boundaries and potentially causing thermal desorption, thereby lowering the internal hydrogen concentration [125]. Additionally, oxide films formed on metal surfaces at high temperatures can inhibit HE [126]. Overall, research on the effects of temperature on HE in commonly used pipeline steels, particularly in hydrogen-enriched natural gas environments, remains limited. Further study is required to understand the impact of seasonal pipeline temperature variations on hydrogen diffusion and aggregation in steel, as well as to determine the safe transportation temperatures for different steels. Synthesizing the available studies, we observe that the relationship between temperature and HE susceptibility is not monotonic and appears to be material-specific. From a research perspective, we emphasize the need for systematic studies that decouple the effects of temperature on hydrogen ingress, trapping, and mechanical response under well-defined conditions.

4.3.3. Stress State

The stress state of pipeline steel, including its strain rate and stress form, influences hydrogen diffusion within the metal, consequently affecting its susceptibility to hydrogen embrittlement (HE). Ilin et al. [127] observed that a lower strain rate correlates with a higher hydrogen concentration in the material, whereas Barrera et al. [128] confirmed that plastic loss escalates as the strain rate decreases. At low strain rates, hydrogen diffusion within the material outpaces dislocation motion, leading to hydrogen accumulation at the dislocation sites. Conversely, at high strain rates, the dislocation motion surpasses hydrogen diffusion, preventing hydrogen accumulation at dense dislocations and inhibiting crack propagation to critical hydrogen concentrations, resulting in unstable crack growth. However, reducing the strain rate does not invariably heighten HE susceptibility; Okayasu et al. [129] noted that high-strength steel specimens with the lowest strain rates did not exhibit the highest HE sensitivity. In summary, it is imperative to elucidate the coupled effects of various factors (e.g., hydrogen charging method, hydrogen environment, pipe strength, and hydrogen partial pressure) and strain rate on pipe HE susceptibility through experimental investigations.

Under the condition of natural gas–hydrogen blending, the pipe is inevitably subjected to external stress. Research has found that after applying external stress to the pre-hydrogen-filled sample, part of the hydrogen in the sample escapes, resulting in a decrease in hydrogen concentration and insignificant hydrogen embrittlement. After dynamic hydrogen filling, the material exhibited obvious brittle fracture characteristics under the action of hydrogen enrichment in the working environment and hydrogen enrichment under stress loading. Under the action of alternating stress, with the increase in alternating frequency, that is, the change in cyclic stress accelerates, the hydrogen permeation current density decreases, at which time more hydrogen accumulates inside the steel, and the growth rate of fatigue cracks increases significantly, thus significantly shortening the remaining life of the steel pipe [130]. Through the cyclic loading/unloading process, hydrogen can be detached from the dislocation (hydrogen trap) and return to a hydrogen-free state, thereby reducing the susceptibility of the material to hydrogen embrittlement [131].

The welding residual stress in pipeline steel welds affects the hydrogen enrichment in the weld, making cracks more likely to initiate and propagate at locations of maximum stress. Welding residual stress exerts a more pronounced influence on the hydrogen diffusion behavior than microstructural inhomogeneity [132], prompting hydrogen to migrate from the base metal and heat-affected zone into the weld [133], thereby elevating the diffusible hydrogen concentration in areas of residual stress concentration. The peak hydrogen concentration in a six-layer circumferential weld of an X80 steel pipeline is 2.6 times that without welding residual stress [134]. The hydrogen embrittlement resistance of pipelines can be improved by optimizing multiple welding procedures, selecting appropriate temperatures, and choosing suitable weld filler materials to alleviate weld residual stress [132]. Stress primarily alters the hydrogen diffusion and permeation behavior by changing the material's internal microstate. Qu [135] found that under strong cathodic interference conditions with current densities of 10–125 $mA \cdot cm^{-2}$, the hydrogen content entering X80 steel is far lower than the average hydrogen content required to induce hydrogen-induced cracking in X80 steel, while applying stress increases the material's hydrogen embrittlement susceptibility. During the elastic phase, hydrogen permeation parameters, including the hydrogen diffusion coefficient and surface hydrogen concentration, are augmented along with the hydrogen trap density. In the early plastic stage, as the number of dislocations increased, the hydrogen trap density increased significantly, leading to a marked increase in the hydrogen concentration, with hydrogen aggregation reducing its permeation rate. When the hydrogen trap density reached saturation in the later plastic stage, extensive dislocation movement formed new hydrogen diffusion paths, causing the hydrogen permeation rate to rise again and stabilize.

4.3.4. The Effect of Pressure with Different Hydrogen Content on Pipeline Steel

(1) The impact of hydrogen pressure in a pure hydrogen milieu was investigated.

Amaro et al. [130,136] performed tensile and fatigue crack growth tests on X52 and X100 steels in a hydrogen setting, revealing that, compared to an air environment, a high-pressure hydrogen environment (13.8 MPa) significantly reduced elongation and toughness in both steels. Specifically, when hydrogen pressure surged from 1.72 MPa to 20.68 MPa, the fatigue crack growth rate of X100 steel doubled, and in some instances, increased by an order of magnitude. Stalheim et al. [137] and San et al. [138,139] assessed the hydrogen embrittlement susceptibility of various X60, X70, and X80 pipeline steels under hydrogen pressures of 5.5–21 MPa. Their findings demonstrated that, relative to an air environment, a 5.5 MPa hydrogen environment markedly reduced the cross-sectional area and fracture toughness of tensile specimens for each pipeline steel, indicating heightened hydrogen embrittlement; however, a further pressure increase to 21 MPa resulted in relatively minor reductions. Moreover, within a broader stress intensity factor range ($\Delta K_{max} > 20$ $MPa \cdot m^{1/2}$), the fatigue crack growth rate of the specimens exhibited minimal change as the hydrogen pressure rose from 5.5 MPa to 21 MPa. Andrew et al. [140] conducted fatigue crack growth tests on X52 and X100 pipeline steels under four hydrogen pressures (1.7, 7, 21, and 48 MPa), revealing that the fatigue crack growth rate in a hydrogen environment was 1–2 orders of magnitude higher than in air, and within a certain stress intensity factor range, the crack growth rate increased with escalating hydrogen pressure.

(2) The influence of the hydrogen partial pressure within a hydrogen-laden environment

In pipelines transporting hydrogen-blended natural gas, the hydrogen partial pressure can be precisely quantified using Equation (3):

$$P_H = \alpha P \quad (3)$$

where P_H denotes the hydrogen partial pressure, α represents the hydrogen doping ratio, and P signifies the total pressure. Clearly, variations in the hydrogen blending ratio and total pressure alter the hydrogen partial pressure accordingly. Nguyen et al. [141] evaluated X70 steel in a methane/hydrogen blend at three typical pressures (hydrogen doping ratios of 0.1%, 0.5%, 1%, 3%, 5%, and 100%) under pressures of 5, 7, and 10 MPa. The findings indicate that the mechanical properties of X70 steel are predominantly influenced by the hydrogen partial pressure rather than the total pressure, as illustrated in Figure 9. For hydrogen-blended natural gas pipelines, the partial pressure of hydrogen within the pipeline is determined by the hydrogen blending ratio when the transmission pressure remains constant.

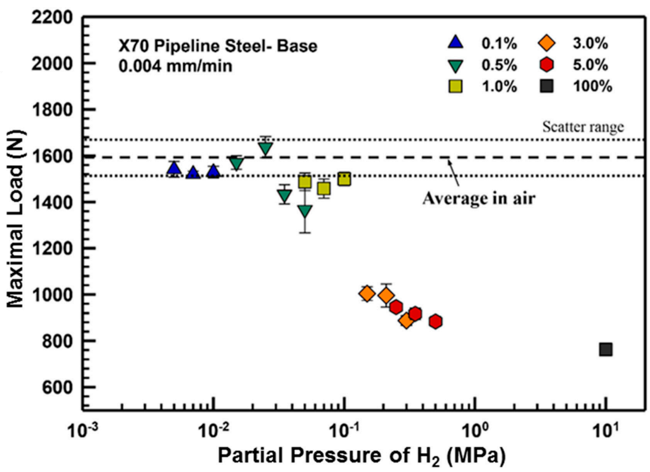

(a)

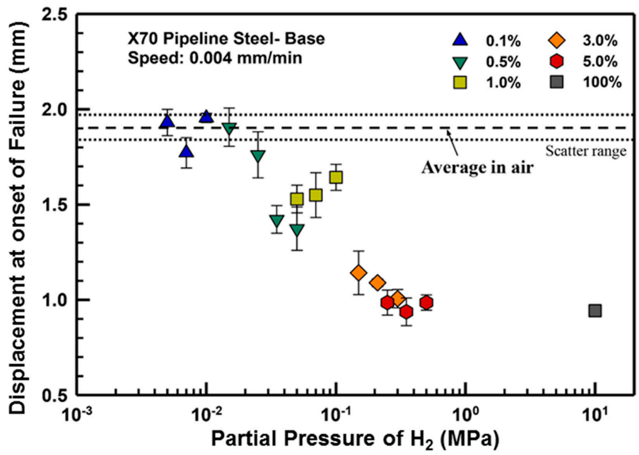

(b)

Figure 9. Influence of partial pressure of hydrogen on X70 steel: (**a**) maximal load; (**b**) displacement at failure onset, reprinted with permission from ref. [50].

4.3.5. Corrosive Environment

Natural gas pipelines, primarily buried, are susceptible to electrochemical corrosion on their outer walls owing to the moist soil environment and microbial byproducts, such as H_2S. Internally, impurities such as H_2S, CO_2, and H_2O accumulate in pits, inducing corrosion. Over extended service, corrosion defects emerge on both surfaces, thinning the walls, concentrating local stress, and reducing the pressure-bearing capacity. Notably, wet H_2S corrodes pipeline steel far more rapidly than wet CO_2, which also triggers hydrogen corrosion. When both impurities coexist, a coupling-competitive effect is evident: initially, CO_2 intensifies H_2S corrosion, but subsequently, corrosion products such as FeS and $FeCO_3$ form a dense film, impeding corrosive solution penetration. Thus, the H_2S/CO_2 partial pressure ratio is pivotal for studying hydrogen-affected pipeline steel corrosion [142].

5. The Impact of Hydrogen Embrittlement on Pipeline Steel Performance and Its Research Methods

5.1. The Effect of Hydrogen on the Plasticity and Toughness of Pipeline Steel

At present, Slow Strain Rate Tensile (SSRT) testing and fracture toughness assessments conducted within gaseous hydrogen constitute the principal approaches for investigating the resistance to hydrogen embrittlement of pipeline steels. The hydrogen embrittlement index (I_E) was calculated using Equation (4):

$$I_E = \frac{L_0 - L_H}{L_0} \tag{4}$$

In the given formula, L_0 and L_H denote the post-fracture elongation of specimens subjected to SSRT in hydrogen-free and hydrogen-containing environments, respectively. Typically, with escalating hydrogen pressure, the hydrogen embrittlement index of X42–X100 pipeline steels exhibit an upward trajectory. Furthermore, the hydrogen embrittlement index is somewhat correlated with pipeline steel strength; higher strength corresponds to heightened susceptibility to hydrogen embrittlement [143–149].

Li et al. [145] subjected X52 pipeline steel to SSRT under 4 MPa total pressure with 0–2 MPa hydrogen, noting unchanged yield and tensile strengths but reduced post-fracture elongation and cross-sectional area, leading to a peak hydrogen embrittlement index of 13%, below the engineering threshold. X70 steel, a widely used high-grade pipeline steel, exhibits low hydrogen embrittlement susceptibility at low hydrogen levels. Guan et al. [150] and Lang et al. [151] found no significant impact on X70 base metal and welds under 0.2–0.36 MPa hydrogen, with fracture toughness degradation within 10%. However, Alvaro et al. [152], Nguyen et al. [13,50] and Shang et al. [153] reported that, at 0.1 MPa hydrogen, X70 base metal plasticity remained unchanged while weld plasticity and fracture toughness decreased significantly. Under high-pressure pure hydrogen ($\geq$10 MPa), X70 steel experienced marked plasticity and toughness degradation. NGUYEN et al. [147] compared X42, X65, and X70 steels under varying hydrogen mixtures and observed brittle fracture in an H_2/CH_4 blend with 30% H_2. With increasing hydrogen content, the post-fracture elongation and cross-sectional area decreased.

Regarding the hydrogen embrittlement behavior of X80 pipeline steel, findings parallel those for X52–X70 grades: adding 0–20% hydrogen to mixed gases minimally affects X80's yield and tensile strengths but reduces its plasticity [154,155]. Moro et al. [156,157] noted that, at 0.1–5.0 MPa hydrogen partial pressure, X80's plasticity decreases significantly with rising pressure; beyond 5 MPa, changes stabilize, and at 10–30 MPa, plasticity remains nearly constant. At 30 MPa, its fracture toughness drops by over 90% compared to that of air. Research on X100 pipeline the hydrogen embrittlement behavior has also been conducted. Nanninga et al. [144] observed that gaseous hydrogen minimally impacts X100's yield and tensile strengths with susceptibility increasing alongside steel strength.

While the SSRT-derived hydrogen embrittlement index (I_e) is widely used for material screening and comparison, a more comprehensive materials design approach requires consideration of fracture mechanics parameters. Key among these is the threshold stress intensity factor for hydrogen-induced cracking (KIH or KTH), which represents the critical stress intensity below which a pre-existing crack will not propagate in a hydrogen environment, and the fatigue crack growth rate and its threshold (ΔKTH), which are essential for life prediction under cyclic loading. Standardized test methods for these parameters are provided in ASTM standards. These fracture mechanics-based metrics provide a more quantitative basis for damage tolerance design and are increasingly emphasized in hydrogen pipeline research.

5.2. Effect of Hydrogen on the Fatigue Performance of Pipeline Steel

The fatigue crack growth rate (FCGR) is a critical metric [158–161]. Hydrogen primarily affects fatigue performance by accelerating fatigue crack initiation and propagation, thereby altering the fatigue life. When the stress intensity factor surpasses a critical threshold contingent upon material properties, hydrogen pressure, and loading conditions, hydrogen can expedite the FCGR.

Metal fatigue typically progresses in three stages: crack initiation, propagation, and fracture. Li et al. [151] demonstrated that, at 0.36 a hydrogen partial pressure, the FCGR of steel was higher than that in air at the heat-affected zone with cleavage fracture surfaces. Ronevich et al. [161] observed significantly higher crack propagation rates under 21 MPa hydrogen compared to air. Drexler et al. [162] found higher FCGRs in the substrate, weld, and heat-affected zone of X52 and X70 pipeline steels in hydrogen-containing environments, although hydrogen pressure had minimal impact on crack propagation rates. Shi et al. [163] studied hydrogen-induced cracking, finding hydrogen accelerates cracking, with X70 and X80 showing good resistance and X90 and X100 exhibiting poorer resistance. Numerous studies indicate that while small amounts of hydrogen significantly increase crack propagation rates in pipeline steel, the accelerating effect diminishes with increasing hydrogen pressure.

5.3. Characterization Methods of Hydrogen in Steel and Development of New Methods

Characterizing the multiscale behavior of hydrogen evolution plays a significant role in the study of hydrogen embrittlement. Among them, slow strain rate tensile testing (SSRT) is a widely used method to determine a material's susceptibility index through changes in its tensile properties. Thermal desorption analysis (TDA) is a pivotal tool for investigating hydrogen atom behavior, enabling the quantitative measurement of hydrogen trap energies and contents, albeit without revealing specific hydrogen distribution states. With advancements in characterization techniques, methods such as hydrogen microcontact printing (HMT), atomic probe tomography (APT), and scanning Kelvin probe force microscopy (SKPFM) have become instrumental in characterizing hydrogen atoms at an advanced level. HMTs are simple to operate and can visualize the diffusion of hydrogen; however, they cannot achieve continuous observation of the hydrogen diffusion kinetics [164]. Researchers investigated the hydrogen diffusion pathways of different grades of pipeline steel through HMT, and the results showed that the grain boundary and phase interface are the main channels for hydrogen diffusion in X65 pipeline steel [165]. In X70 pipeline steel, carburite is the easiest path for hydrogen diffusion [166]. APT is one of the testing techniques with the highest available spatial resolution [167], which is essential for understanding the distribution and behavior of hydrogen in materials. For example, high-resolution three-dimensional distribution through APT shows that carbides in ferrite can be an effective trap for hydrogen [168]. Takahashij et al. [169] directly observed the hydrogen capture site of the TiC precipitated phase in steel at the atomic scale using APT and found that the interface between the substrate and TiC is the main capture site for hydrogen. Although APT can achieve resolution of the three-dimensional spatial distribution of atoms/precipitated phases, the cost of APT sample preparation and detection is high, and it is still difficult to popularize [164]. The principle of SKPFM is to reveal the hydrogen distribution by detecting the change in the contact potential difference between the probe and sample, such as the hydrogen capture behavior at the interface of the non-crystalline nanoprecipitated phase [170]. The test process is shown in Figure 10. The results show that not all non-colloidal interfaces can capture hydrogen, and some may even repel hydrogen.

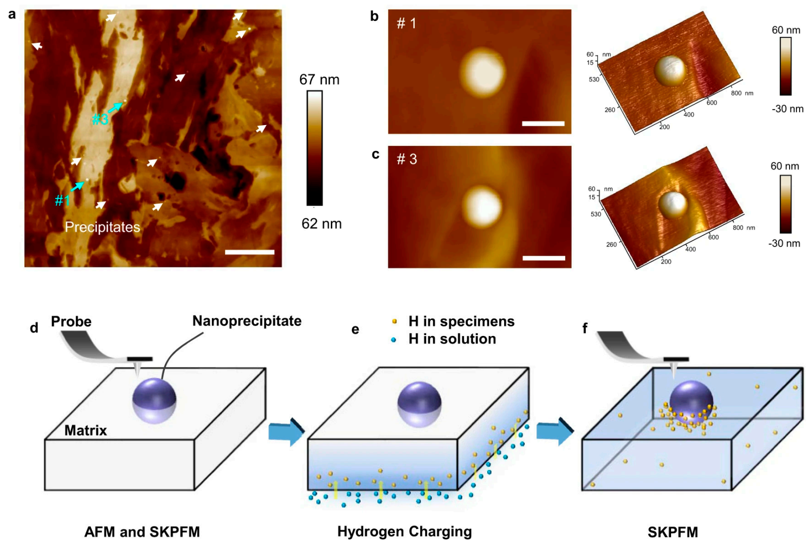

Figure 10. Atomic force microscopy (AFM) and experimental process of precipitated phase in martensite substrate: (**a**) Topography map for martensite matrix including nanoprecipitates. (**b**,**c**) Tomography maps of precipitate #1 and #3 corresponding to marked by the cyan arrows in panel (**a**) respectively. (**d**–**f**) Schematic illustrations of the scanning Kelvin probe force microscopy (SKPFM) experiment procedure. Reprinted from Ref. [170].

Advances in computational science have made machine learning (ML) an essential tool for analyzing the relationship between material properties and properties. Remarkable results have been achieved through ML-assisted design of anti-hydrogen embrittlement materials [171]. For instance, leveraging data-driven and machine learning (ML) approaches, the quantitative correlation between the hydrogen diffusion coefficient and chemical composition was unveiled. The combination of ML and first-principles calculations can also assist in the design of anti-hydrogen embrittlement materials, such as by proposing new methods to study and predict the diffusivity of hydrogen based on ML and first-principles, which has certain guiding significance for comprehending and improving the hydrogen embrittlement resistance of materials [172]. Some researchers used deep neural networks with Bayesian optimization to accurately predict the FCGR of AISI4140 alloys under hydrogen-induced embrittlement scenarios [173,174]. Zhang et al. [175] introduced a hybrid approach integrating physical principles with ensemble learning to predict the fracture toughness, demonstrating superior predictive accuracy compared to random forests and extreme gradient boosting. Shi et al. [176] undertook a cross-scale study encompassing atomic-scale observation, theoretical computations, and macroscopic performance testing, revealing that deep hydrogen traps at the semi-coherent NbC/α-Fe interface facilitate the design of high-strength steels with exceptional resistance to hydrogen embrittlement. As illustrated in

Figure 11, a multiscale computational framework holds immense potential for constructing a hydrogen embrittlement prediction system spanning from atomic to macroscopic scales by integrating atomic-scale density functional theory (DFT) calculations, nanoscale molecular dynamics (MD) simulations, micron-scale dislocation dynamics (hydrogen-dislocation interactions), and macroscopic models (microstructure-performance correlations) [177].

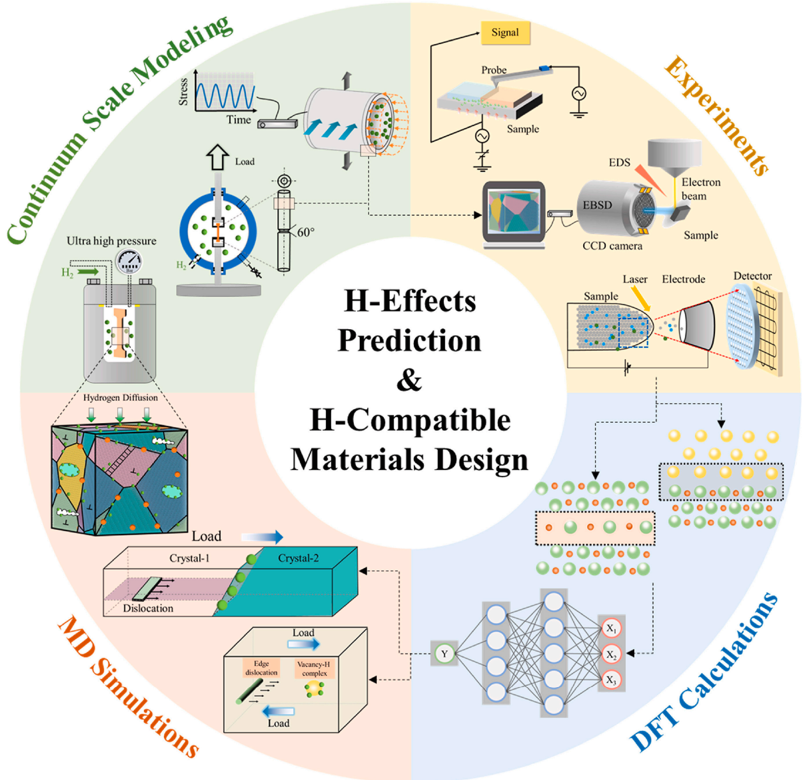

Figure 11. Schematics of cross-scale research, reprinted with permission from ref. [177].

6. Measures to Prevent Hydrogen Embrittlement

6.1. Changing the Microstructure

Owing to the significant differences in hydrogen embrittlement sensitivity among different microstructural metallographies, an ideal microstructure can be achieved by optimizing the heat treatment processes and parameters, and grain refinement processes can also improve the steel's resistance to hydrogen embrittlement [178]. Enyinnaya et al. [179] comparatively study on the hydrogen embrittlement resistance of X70 pipeline steel with distinct phase structures, revealing that X70 steel with a higher martensite/residual austenite content exhibited superior resistance to hydrogen-induced cracking. Similarly, Ohaeri et al. [180] subjected X70 steel to a two-step annealing process, which resulted in a ferrite-tempered martensite dual-phase structure. Despite the reduction in strength, the finer grain size of the tempered martensite retarded hydrogen migration within the steel. Park et al. [181] assessed the hydrogen embrittlement resistance of X65 steel subjected to various heat treatments, finding that the high toughness of acicular ferrite hindered crack propagation increased with acicular ferrite content. However, altering the phase structure may lead to a partial decline in the mechanical properties, and process control is complex and energy-intensive [182]. Whether this method can be applied on a large scale to long-distance pipeline steels in the future remains to be verified.

6.2. Gas Suppressants

In recent scholarly pursuits, investigators have discovered that the incorporation of supplementary gases into a system can effectively mitigate the challenge of hydrogen embrittlement. Shang et al. [183] found that mild steel adsorbs CO_2 in natural gas, and the interaction between CO_2 and H_2 accelerates the crack propagation of metals. Meng et al. [184] found that X80 pipeline steel is sensitive to methane and H_2 mixtures, and the sensitivity increases with an increase in hydrogen composition. Michler et al. [185] conducted an in-depth investigation into the impact of O_2 on the susceptibility of high-strength pearlitic and austenitic steels to hydrogen embrittlement. Their findings revealed that the partial pressure of oxygen emerged as the principal factor governing its suppressive influence. Somerday et al. [186] examined the influence of O_2, observing that the initial FCGRs in high-purity hydrogen and hydrogen-oxygen mixtures were comparable, followed by abrupt crack acceleration as the stress intensity factor range (ΔK) increased. Notably, the critical ΔK threshold for accelerated crack propagation increased with increasing oxygen content in the mixture.

6.3. Hydrogen-Blocking Coating

Increasing the physical barriers by depositing coatings on the metal surface can significantly reduce the hydrogen embrittlement behavior of metals. Coatings include oxide layers such as Al_2O_3, TiO_2, and Cr_2O_3; electroplated layers such as Ni, Cd, and Sn; and sprayed layers such as TiC, TiN, BN, and WC. The process of selecting suitable coatings on the surface of a material for protection aims to block or reduce the penetration of external hydrogen into the material. This includes reducing the surface activity of the material to lower the decomposition rate of hydrogen on the material's exterior and inhibiting the diffusion of hydrogen atoms or ions within the coating. Shi et al. [187] injected carbon into a pre-deposited nickel catalytic layer on the surface of tubular steel, followed by annealing to segregate and form multilayer graphene. The SSRT results showed that this coating exhibits excellent resistance to hydrogen embrittlement because the coating suppresses hydrogen evolution, elongates diffusion paths, reduces the permeation area, and enhances hydrogen adsorption, thereby reducing the hydrogen content entering the material under the same external conditions and mitigating hydrogen damage. However, coatings also have certain defects, such as pores and microcracks, which can serve as fast channels for the ingress of hydrogen atoms and generate hydrogen-induced cracks. Shot peening can also improve HE resistance. As discussed in Section 4.2.7, the residual compressive stress generated by shot peening delays crack initiation and hinders crack propagation by counteracting tensile stresses that drive hydrogen accumulation [188]. Shot peening increased the energy required for crack initiation and suppressed the propagation of pre-existing cracks within the specimen.

Al_2O_3 has a good hydrogen barrier effect in metal-oxide coatings. A 1 μm thick Al_2O_3 layer can reduce hydrogen permeation flux by three to four orders of magnitude, and it also maintains good stability at high temperatures [189,190]. Compared to single-layer oxide coatings, composite coatings exhibit better hydrogen barrier performance, stronger adhesion, and greater stability [191,192]. However, not all oxides act as effective hydrogen barriers. Their influence on hydrogen embrittlement largely depends on the depth distribution, grain size, and packing method of oxide. Only specific oxide layers exhibit good hydrogen-blocking effects [193]. With the rise in graphene materials, research on their hydrogen barrier properties has received widespread attention in recent years. When hydrogen atoms enter a graphene coating, C-H sp3 bonds are formed, which hinder hydrogen permeation. Covering the metal surface with graphene coating can significantly reduce the hydrogen content of the metal [194]. The formation of C-H bonds causes deformation of the graphene structure, reducing its hydrogen barrier capability. By adjusting the synthesis method to further reduce the grain size, improve the graphene structure, and develop multilayer graphene, the anti-deformation ability of graphene coatings can be further enhanced [195].

Although coatings have good hydrogen barrier properties, the coating itself can introduce some hydrogen atoms during processing, and once damaged, it can cause severe localized corrosion. In addition, owing to economic considerations and limitations in processing technology, hydrogen barrier coatings cannot be applied on a large scale. Current research mainly uses liquid-phase hydrogen charging experiments to evaluate the effectiveness of hydrogen barrier coatings, which cannot accurately reflect their performance in hydrogen gas environments. Further studies are required to assess their resistance to hydrogen embrittlement under high-pressure gas conditions. Moreover, the effectiveness of new coating materials and novel coating preparation processes requires further investigation.

6.4. Controlling Hydrogen Doping Amount

The hydrogen charging duration, method, and storage period of pipeline steel induce variations in the hydrogen content, subsequently influencing its hydrogen embrittlement susceptibility [196]. Zhang et al. [14] explored the correlation between hydrogen partial pressure and the fatigue life, unveiling that elevated hydrogen partial pressure enhances the steady-state hydrogen permeation current density, consequently leading to a reduction in the pipeline steel's operational lifespan. According to the HEDE theory, hydrogen diminishes the interatomic bonding strength. Consequently, Wei et al. [197] and Zhang et al. [198] posited that the crack propagation rate in X80 steel under hydrogen is contingent upon hydrogen pressure; greater hydrogen accumulation at the crack tip reduces the interatomic bonding strength [199].

6.5. Optimize Environmental Temperature

Some researchers believe that an increase in temperature will accelerate the diffusion of hydrogen and reduce the dislocation hydrogen capture capacity, and the hydrogen concentration will not reach the critical value [200]. Xu et al. [201] conducted an in-depth investigation, revealing that elevated temperatures markedly accelerated hydrogen diffusion rates. Xing et al. [123] systematically examined the interplay between hydrogen embrittlement and temperature, demonstrating that the critical threshold temperature of hydrogen embrittlement in X90 steel is 313 K. Notably, beyond this threshold, the hydrogen embrittlement susceptibility exhibits an inverse relationship with temperature, whereas below this threshold, a direct proportionality is observed.

7. Conclusions and Future Perspectives

This review has systematically examined the current understanding of hydrogen embrittlement in pipeline steels for hydrogen transport, spanning fundamental mechanisms, influencing factors, performance implications, characterization methods, and mitigation strategies. Synthesizing the literature, we identify several overarching themes and key challenges that define the current landscape and future trajectory of the field:

(1) The multi-mechanism nature of HE is now widely recognized, with HEDE, HELP, and HESIV likely operating synergistically rather than in isolation. However, the precise conditions under which each mechanism dominates, and how they interact at crack tips and microstructural interfaces, remain poorly understood. From our perspective, advancing this understanding requires integrated experimental-computational approaches that combine high-resolution characterization (e.g., in situ TEM, APT) with multi-scale modeling (DFT, MD, phase-field).

(2) The susceptibility of pipeline steel to HE is determined by a complex interplay of intrinsic material factors and extrinsic service conditions. A recurring theme throughout this review is the importance of interactions—for example, between hydrogen pressure and microstructure, or between temperature and dislocation dynamics. We suggest that future research should move beyond studying individual factors in isolation and instead focus on systematic investigation of these interactions under well-defined, application-relevant conditions.

(3) While significant progress has been made in characterizing HE and developing mitigation strategies, critical gaps remain in translating this knowledge into engineering practice. These include: the need for standardized testing protocols and design codes that incorporate fracture mechanics parameters; the lack of comprehensive, publicly accessible databases linking material properties, processing history, service conditions, and HE performance; and the challenge of scaling laboratory findings to long-term pipeline operation under realistic conditions.

Looking forward, we envision that the integration of data-driven approaches (e.g., machine learning trained on high-quality datasets) with physics-based models will accelerate the discovery and design of HE-resistant materials. Furthermore, grain boundary engineering and precipitate engineering offer promising pathways for creating microstructures that inherently manage hydrogen distribution. Finally, we emphasize the importance of coordinated development of hydrogen blending and pure hydrogen pipeline technologies to enable the gradual but robust construction of a hydrogen energy infrastructure. We hope this review provides a useful foundation for researchers and engineers working toward this critical goal.

Funding: This work was financially supported by Science and Technology Program of Karamay City (Grant No. 2024hjcxrc0088), Foundation at Karamay Vocational & Technical College, (KZY2024-1), Jiangsu Key Laboratory of Oil-Gas & New-Energy and Transportation Technology (OGNETT-2402).

Data Availability Statement: No new data were created or analyzed in this study. Data sharing is not applicable to this article.

Conflicts of Interest: The authors declare no conflict of interest.

References

1. Qiu, Y.; Zhou, S.Y.; Gu, W.; Pan, G.S.; Chen, X.G. Application Prospect Analysis of Hydrogen Enriched Compressed Natural Gas Technologies under the Target of Carbon Emission Peak and Carbon Neutrality. *Proc. CSEE* **2022**, *42*, 1301–1321. [CrossRef]
2. Deepthi, J.K.; Praveen, K.K. Advances in solar-powered hydrogen energy generation, storage and applications. *Int. J. Hydrogen Energy* **2026**, *199*, 152816. [CrossRef]
3. Chowdhury, M.F.W.; Tapia-Bastidas, C.V.; Hoschke, J.; Venezuela, J.; Atrens, A. A Review of Influence of Hydrogen on Fracture Toughness and Mechanical Properties of Gas Transmission Pipeline Steels. *Int. J. Hydrogen Energy* **2025**, *102*, 181–221. [CrossRef]
4. Simonas, C.; Antonio, J.C.J.; Thomas, G.; Martin, R.; Detlef, S. Options of natural gas pipeline reassignment for hydrogen: Cost assessment for a Germany case study. *Int. J. Hydrogen Energy* **2020**, *45*, 12095–12107. [CrossRef]
5. Li, Q.Y.; Zhao, M.H.; Zhang, B.; Wen, W.; Wang, L.L.; Zhang, X.Q.; Chen, L. Current Construction Status and Development Trend of Global Oil and Gas Pipelines in 2020. *Oil Gas Storage Transp.* **2021**, *40*, 1330–1337.
6. Andrzej, W.; Andrzej, R.; Mirosław, M.; Katarzyna, S. Analysis of Compression and Transport of the Methane/Hydrogen Mixture in Existing Natural Gas Pipelines. *Int. J. Press. Vessel. Pip.* **2018**, *166*, 24–34. [CrossRef]
7. Hoschke, J.; Chowdhury, M.F.W.; Venezuela, J.; Atrens, A. A Review of Hydrogen Embrittlement in Gas Transmission Pipeline Steels. *Corros. Rev.* **2023**, *41*, 277–317. [CrossRef]
8. Zou, S.J.; Chen, H.; Zhou, Y.; Wang, W.; Song, T.J.; Wang, S.Q.; Zhu, X.Y.; Sang, B.G. Hydrogen Diffusion and Hydrogen Embrittlement Susceptibility of Cu-Containing Maraging Stainless Steel. *Met. Mater. Int.* **2026**, *32*, 298–313. [CrossRef]
9. Liu, Z.; Li, Y.; Song, W.C.; Xin, M. Effect of Hydrogen Content and Loading Frequency on Fatigue Crack Growth Rate of X80 Steel Pipe Joint. *Mater. Mech. Eng.* **2024**, *48*, 51–56. [CrossRef]

10. Nagumo, M.; Takai, K. The predominant role of strain-induced vacancies in hydrogen embrittlement of steels: Overview. *Acta Mater.* **2019**, *165*, 722–733. [CrossRef]
11. Wang, J.; Atrens, A. Analysis of Service Stress Corrosion Cracking in a Natural Gas Transmission Pipeline, Active or Dormant. *Eng. Fail. Anal.* **2004**, *11*, 3–18. [CrossRef]
12. Djukic, M.B.; Bakic, G.M.; Zeravcic, V.S.; Sedmak, A.; Rajicic, B. The synergistic action and interplay of hydrogen embrittlement mechanisms in steels and iron: Localized plasticity and decohesion. *Eng. Fract. Mech.* **2019**, *216*, 106528. [CrossRef]
13. Alvaro, A.; Wan, D.; Olden, V.; Barnoush, A. Hydrogen enhanced fatigue crack growth rates in a ferritic Fe-3 wt%Si alloy and a X70 pipeline steel. *Eng. Fract. Mech.* **2019**, *219*, 106641. [CrossRef]
14. Zhang, S.; Li, J.; An, T.; Zheng, S.Q.; Yang, K.; Lv, L.; Xie, C.; Chen, L.Q.; Zhang, L. Investigating the influence mechanism of hydrogen partial pressure on fracture toughness and fatigue life by in situ hydrogen permeation. *Int. J. Hydrogen Energy* **2021**, *46*, 20621–20629. [CrossRef]
15. Jubica; Claeys, L.; Laureys, A.; De Waele, W.; Schweicher, J.; Depover, T.; Verbeken, K. Gaseous Inhibitors: A Comprehensive Overview on Mitigating Hydrogen Embrittlement in Pipeline Steels. *Int. J. Hydrogen Energy* **2025**, *136*, 630–642. [CrossRef]
16. Sun, Y.H.; Cheng, Y.F. Thermodynamics of spontaneous dissociation and dissociative adsorption of hydrogen molecules and hydrogen atom adsorption and absorption on steel under pipelining conditions. *Int. J. Hydrogen Energy* **2021**, *46*, 34469–34486. [CrossRef]
17. Xing, Y.Y.; Yang, Z.L.; Yao, X.C.; Wang, X.Y.; Lu, M.X.; Zhang, L.L.; Qiao, J. Effects of hydrogen on the fracture toughness of X80 steel base metal and girth weld under strong cathodic current with in situ hydrogen charging. *Eng. Fail. Anal.* **2022**, *135*, 106143. [CrossRef]
18. Zhu, S.D.; Li, Y.L.; Cao, P.C.; Liao, Y.G.; Cao, F.; Li, G. Research Progress on Hydrogen Embrittlement Sensitivity of Pipeline Steel for Hydrogen-Blended Natural Gas Transportation. *Mater. Mech. Eng.* **2025**, *49*, 12–24. [CrossRef]
19. Praswanto, D.H.; Djiwo, S.; Palevi, B.R.P.D. Analysis of hydrogen gas production results in water electrolysis process on genset characteristics. *J. Sci. Appl. Eng.* **2023**, *6*, 50. [CrossRef]
20. Johnson, W.H. On some remarkable changes produced in iron and steel by the action of hydrogen and acids. *Nature* **1875**, *11*, 393. [CrossRef]
21. Yang, F.Y.; Wang, T.Z.; Deng, X.T.; Dang, J.; Huang, Z.Y.; Hu, S.; Li, Y.Y.; Ouyang, M.G. Review on hydrogen safety issues: Incident statistics, hydrogen diffusion, and detonation process. *Int. J. Hydrogen Energy* **2021**, *46*, 31467–31488. [CrossRef]
22. Yazdani, T.; Soni, A.; Vishwakarma, M. Hydrogen embrittlement in aluminium alloys under electrochemical charging: Tensile property degradation, failure mechanisms, and prevention strategies. *Eng. Fail. Anal.* **2026**, *184*, 110294. [CrossRef]
23. Chung, Y.; Fulton, L.K. Environmental Hydrogen Embrittlement of G41400 and G43400 Steel Bolting in Atmospheric Versus Immersion Services. *J. Fail. Anal. Prev.* **2017**, *17*, 330–339. [CrossRef]
24. Gorman, J.A.; Gross, D.; Hall, T.S.; Matty, S.; Christoffersen, S.A.; Cavendish, T.; Robert, S. San Francisco-Oakland Bay Bridge anchor rod cracking issues. *Mater. Perform.* **2015**, *54*, 52–57. [CrossRef]
25. Lynch, S.P. 2-Hydrogen Embrittlement (HE) Phenomena and Mechanisms. In *Stress Corrosion Cracking*; Raja, V.S., Shoji, T., Eds.; Woodhead Publishing: Cambridge, UK, 2011; pp. 90–130. [CrossRef]
26. Dwivedi, S.K.; Vishwakarma, M. Effect of hydrogen in advanced high strength steel materials. *Int. J. Hydrogen Energy* **2019**, *44*, 28007–28030. [CrossRef]
27. Huang, C.; Cui, C.J.; Niu, R.M.; Lu, F.H.; Wu, C.Y.; Zhu, X.X.; Lu, H.Z.; Zhang, Y.Q.; Liu, P.Y.; Dong, B.S.; et al. Strong hydrogen trapping by tangled dislocations in cold-drawn pearlitic steels. *Acta Mater.* **2025**, *296*, 121231. [CrossRef]
28. Oriani, R.A.; Josephic, P.H. Equilibrium aspects of hydrogen-induced cracking of steels. *Acta Metall.* **1974**, *22*, 1065–1074. [CrossRef]
29. Blanchard, P.A.; Troiano, A.R. Embrittlement of metals by hydrogen. Influence of the crystallographic and electronic structure. *Trans. Am. Soc. Met.* **1960**, *52*, 54–80.
30. Oriani, R.A. A mechanistic theory of hydrogen embrittlement of steels. *Berichte Bunsenges. Phys. Chem.* **1972**, *76*, 848–857. [CrossRef]
31. Pfeil, L.B. The effect of occluded hydrogen on the tensile strength of iron. *Proc. A* **1926**, *112*, 182–195. [CrossRef]
32. Jiang, D.E.; Carter, E.A. First principles assessment of ideal fracture energies ofmaterials with mobile impurities; implications for hydrogen embrittlement of metals. *Acta Mater.* **2004**, *52*, 4801–4807. [CrossRef]
33. Pezold, J.V.; Lymperakis, L.; Neugebeauer, J. Hydrogen-enhanced local plasticity at dilute bulk H concentrations: The role of H–H interactions and the formation of local hydrides. *Acta Mater.* **2011**, *59*, 2969–2980. [CrossRef]
34. Lu, G.; Zhang, Q.; Kioussis, N.; Kaxiras, E. Hydrogen-enhanced local plasticityin aluminum: An ab initio study. *Phys. Rev. Lett.* **2001**, *87*, 095501. [CrossRef]
35. Ferreira, P.J.; Robertson, I.M.; Birnbaum, H.K. Hydrogen effects on theinteraction between dislocations. *Acta Mater.* **1998**, *46*, 1749–1757. [CrossRef]

36. Zhao, K.; He, J.Y.; Mayer, A.E.; Zhang, Z.L. Effect of hydrogen on the collective behavior of dislocations in the case of nanoindentation. *Acta Mater.* **2018**, *148*, 18–27. [CrossRef]
37. Tabata, T.; Birnbaum, H.K. Direct observations of the effect of hydrogen on the behavior of dislocations in iron. *Scr. Metall.* **1983**, *17*, 947–950. [CrossRef]
38. Nagumo, M.; Nakamura, M.; Takai, K. Hydrogen thermal desorption relevant to delayed-fracture susceptibility of high-strength steels. *Metall. Mater. Trans. A* **2001**, *32*, 339–347. [CrossRef]
39. Kirchheim, R. Reducing grain boundary, dislocation line and vacancy formation energies by solute segregation. I. Theoretical background. *Acta Mater.* **2007**, *55*, 5129–5138. [CrossRef]
40. Saito, K.; Hirade, T.; Takai, K. Hydrogen Desorption Spectra from Excess Vacancy-Type Defects Enhanced by Hydrogen in Tempered Martensitic Steel Showing Quasi-cleavage Fracture. *Metall. Mater. Trans. A* **2019**, *50*, 5091–5102. [CrossRef]
41. Li, L.L.; Kamachali, R.D.; Li, Z.M.; Zhang, Z.F. Grain boundary energy effect on grain boundary segregation in an equiatomic high-entropy alloy. *Phys. Rev. Mater.* **2020**, *4*, 053603. [CrossRef]
42. Li, Q.; Mo, J.W.; Ma, S.H.; Duan, F.H.; Zhao, Y.L.; Liu, S.F.; Liu, W.H.; Zhao, S.J.; Liu, C.T.; Liaw, P.K.; et al. Defeating hydrogen-induced grain-boundary embrittlement via triggering unusual interfacial segregation in FeCrCoNi-type high-entropy alloys. *Acta Mater.* **2022**, *241*, 118410. [CrossRef]
43. Kirchheim, R. Hydrogen solubility and diffusivity in defective and amorphous metals. *Prog. Mater. Sci.* **1988**, *32*, 261–325. [CrossRef]
44. Wei, H.T.; Tang, H.; Xing, B.H.; Shang, J.; Qiu, S.Y.; Hua, Z.L.; Gu, C.H. Research on the fracture toughness of pipeline steel X80 in a hydrogen environment. *Eng. Fail. Anal.* **2025**, *180*, 109917. [CrossRef]
45. Briottet, L.; Moro, I.; Lemoine, P. Quantifying the hydrogen embrittlement of pipeline steels for safety considerations. *Int. J. Hydrogen Energy* **2012**, *37*, 17616–17623. [CrossRef]
46. Hardie, D.; Charles, E.A.; Lopez, A.H. Hydrogen embrittlement of high strength pipeline steels. *Corros. Sci.* **2006**, *48*, 4378–4385. [CrossRef]
47. Islam, A.; Alam, T.; Sheibley, N.; Edmonson, K.; Burns, D.; Hernandez, M. Hydrogen blending in natural gas pipelines: A comprehensive review of material compatibility and safety considerations. *Int. J. Hydrogen Energy* **2024**, *93*, 1429–1461. [CrossRef]
48. Chang, B.; Luo, Y.; Zhang, C.Y.; Zhang, Z.Y.; Liu, C.X.; Liu, Y.C. Enhancing sulfide stress cracking resistance of 125 ksi high-strength steel via double quenching and tempering. *Corros. Sci.* **2026**, *264*, 113741. [CrossRef]
49. Nguyen, T.T.; Beak, U.B.; Park, J.; Nahm, S.H.; Tak, N. Hydrogen environment assisted cracking in X70 welding heat-affected zone under a high-pressure hydrogen gas. *Theor. Appl. Fract. Mech.* **2020**, *109*, 102746. [CrossRef]
50. Nguyen, T.T.; Park, J.; Kim, W.S.; Nahm, S.H.; Beak, U.B. Effect of low partial hydrogen in a mixture with methane on the mechanical properties of X70 pipeline steel. *Int. J. Hydrogen Energy* **2020**, *45*, 2368–2381. [CrossRef]
51. Feng, J.G.; Li, J.L.; Fan, Q.S.; Jiang, J.D.; Zhang, Z.Y.; Li, J.H.; Qin, C.K. Study on corrosion of X80 steel under dynamic stray current interference based on hybrid experimental -data-driven approach. *Constr. Build. Mater.* **2026**, *511*, 145339. [CrossRef]
52. Zhang, L.; Shen, H.J.; Lu, K.D.; Cao, W.H.; Sun, Y.N.; Fang, Y.C.; Xing, Y.Y.; Du, Y.X.; Lu, M.X. Investigation of hydrogen concentration and hydrogen damage on API X80 steel surface under cathodic overprotection. *Int. J. Hydrogen Energy* **2017**, *42*, 29888–29896. [CrossRef]
53. Marques, S.C.; Castilho, A.V.; Santos, D.S.D. Effect of alloying elements on the hydrogen diffusion and trapping in high entropy alloys. *Scr. Mater.* **2021**, *201*, 113957. [CrossRef]
54. Cho, H.J.; Cho, Y.; Kim, S.J. Hydrogen embrittlement susceptibility of Cu bearing cost-effective austenitic stainless steels. *Int. J. Hydrogen Energy* **2024**, *60*, 1–10. [CrossRef]
55. Ito, K.; Tanaka, Y.; Tsutsui, K.; Omura, T. Effect of Mo addition on hydrogen segregation at a-Fe grain boundaries: A first-principles investigation of the mechanism by which Mo addition improves hydrogen embrittlement resistance in high-strength steels. *Comput. Mater. Sci.* **2023**, *218*, 111951. [CrossRef]
56. Haq, A.J.; Muzaka, K.; Dunne, D.P.; Calka, A.; Pereloma, E.V. Effect of microstructure and composition on hydrogen permeation in X70 pipeline steels. *Int. J. Hydrogen Energy* **2013**, *38*, 2544–2556. [CrossRef]
57. Vercruysse, F.; Claeys, L.; Depover, T.; Verleysen, P.; Petrov, R.H.; Verbeken, K. The effect of Nb on the hydrogen embrittlement susceptibility of Q&P steel under static and dynamic loading. *Mater. Sci. Eng. A* **2022**, *852*, 143652. [CrossRef]
58. Pampa, G.; Ram, R. Effects of Composition and Coiling Temperature on Precipitation and Texture Formation in a Few Interstitial Free High Strength Steels. In *Materials Processing and Texture*; John Wiley & Sons: Hoboken, NJ, USA, 2008; pp. 151–159. [CrossRef]
59. Ohaeri, E.; Eduok, U.; Szpunar, J. Hydrogen related degradation in pipeline steel: A review. *Int. J. Hydrogen Energy* **2018**, *43*, 14584–14617. [CrossRef]
60. Mohrbacher, H. Application of Microalloying for Controlling Recrystallization and Grain Growth During Downstream Steel Processing. *Metall. Mater. Trans. A* **2026**. [CrossRef]
61. Boot, T.; Kömmelt, P.; Brouwer, H.J.C. Effect of titanium and vanadium nano-carbide size on hydrogen embrittlement of ferritic steels. *npj Mater. Degrad.* **2025**, *9*, 2. [CrossRef]

62. Shi, X.; Yan, W.; Wang, W.; Shan, Y.; Yang, K. Hydrogen-induced cracking resistance of novel cu-bearing pipeline steels. *Acta Metall. Sin.* **2018**, *54*, 1343–1349. [CrossRef]
63. Yoo, J.; Jo, M.C.; Kim, D.W.; Song, H.; Koo, M.; Sohn, S.S.; Lee, S. Effects of Cu addition on resistance to hydrogen embrittlement in 1 GPa-grade duplex lightweight steels. *Acta Mater.* **2020**, *196*, 370–383. [CrossRef]
64. Li, L.F.; Song, B.; Cai, Z.Y.; Liu, Z.; Cui, X.K. Effect of vanadium content on hydrogen diffusion behaviors and hydrogen induced ductility loss of X80 pipeline steel. *Mater. Sci. Eng. A* **2019**, *742*, 712–721. [CrossRef]
65. Yang, X.F.; Yu, H.; Song, C.H.; Li, L.L. Hydrogen trapping behavior in vanadium microalloyed TRIP assisted annealed martensitic steel. *Metals* **2019**, *9*, 741. [CrossRef]
66. Dong, F.T.; Venezuela, J.; Li, H.X.; Shi, Z.M.; Zhou, Q.J.; Chen, L.S.; Chen, J.; Du, L.X.; Atrens, A. Effect of vanadium and rare earth microalloying on the hydrogen embrittlement susceptibility of a Fe-18Mn-0.6C TWIP steel studied using the linearly increasing stress test. *Corros. Sci.* **2021**, *185*, 109440. [CrossRef]
67. Fu, Y.; Li, T.; Yan, Y.B.; Wang, X.Y.; Zhu, M.L.; Xuan, F.Z. A first principles study on H-atom interaction with bcc metals. *Int. J. Hydrogen Energy* **2023**, *48*, 9911–9920. [CrossRef]
68. Zhang, L.Y.; Zhang, Q.Z.; Jiang, P.; Liu, Y.; Zhao, C.; Dong, Y.H. Effects of Alloying Element on Hydrogen Adsorption and Diffusion on α-Fe(110) Surfaces: First Principles Study. *Metals* **2024**, *14*, 487. [CrossRef]
69. Zhang, S.Q.; Qi, L.M.; Liu, S.L.; Peng, Z.X.; Cheng, Y.F.; Huang, F.; Liu, J. Synergistic effects of Nb and Mo on hydrogen-induced cracking of pipeline steels: A combined experimental and numerical study. *J. Mater. Sci. Technol.* **2023**, *158*, 156–170. [CrossRef]
70. Yin, X.P.; Wu, C.X.; Jiang, X.J.; Gao, Z.L. Hydrogen Embrittlement Resistance and Influence Factors of 34CrMo4 Steel for High Pressure Cylinder. *Mater. Mech. Eng.* **2018**, *42*, 23–27,32. [CrossRef]
71. Zhang, S.Q.; Zhao, Q.Y.; Liu, J.; Huang, F.; Huang, Y.H.; Li, X.G. Understanding the effect of niobium on hydrogen-induced blistering in pipeline steel: A combined experimental and theoretical study. *Corros. Sci.* **2019**, *159*, 108142. [CrossRef]
72. Chen, Y.S.; Huang, C.; Liu, P.Y.; Yen, H.W.; Niu, R.M.; Burr, P.; Moore, K.L.; Martínez-Pañeda, E.; Atrens, A.; Cairney, J.M. Hydrogen trapping and embrittlement in metals—A review. *Int. J. Hydrogen Energy* **2025**, *136*, 789–821. [CrossRef]
73. Yagodzinskyy, Y.; Todoshchenko, O.; Saukkonen, T.; Hänninen, H. Role of non-metallic inclusions in hydrogen-induced fracture of high-strength carbon steels. *Metall. Mater. Trans. A* **2014**, *45*, 4742–4747.
74. Javeria, U.; Kim, S.J. Investigation of hydrogen embrittlement in steel alloys: Mechanism, factors, advanced methods and materials, applications, challenges, and future directions: A review. *J. Mater. Res. Technol.* **2025**, *38*, 1276–1301. [CrossRef]
75. Alp, T.; Dames, T.J.; Dogan, B. The effect of microstructure in the hydrogen embrittlement of a gas pipeline steel. *J. Mater. Sci.* **1987**, *22*, 2105. [CrossRef]
76. Nagao, A.; Smith, C.D.; Dadfarnia, M.; Sofronis, P.; Robertson, I.M. The role of hydrogen in hydrogen embrittlement fracture of lath martensitic steel. *Acta Mater.* **2012**, *60*, 5182–5189. [CrossRef]
77. Rodoni, E.; Verbeken, K.; Depover, T.; Iannuzzi, M. Effect of microstructure on the hydrogen embrittlement, diffusion, and uptake of dual-phase low alloy steels with varying ferrite-martensite ratios. *Int. J. Hydrogen Energy* **2024**, *50*, 53–65. [CrossRef]
78. Li, X.; Wei, B.X.; Lu, Y.H.; Sun, C.; Yu, W.T.; Xu, M.; Liu, W. Research Progress on Hydrogen Damage Mechanism of Pipeline Steel in Contact with Hydrogen Environment. *J. Chin. Soc. Corros. Prot.* **2024**, *44*, 1125–1133. [CrossRef]
79. Xing, X.; Wang, C.H.; Liu, J.G.; Cui, G.; Cheng, Y.F.; Zhang, H. Effects of alloy elements on the hydrogen adsorption behavior of pipeline steel: A review. *Renew. Sustain. Energy Rev.* **2025**, *222*, 116003. [CrossRef]
80. Li, M.F.; Zhang, H.; Henein, H.; Liu, J. Hydrogen trapping in precipitates of high-strength steel: Insights into various coherent and stress conditions. *Int. J. Hydrogen Energy* **2024**, *92*, 1356–1365. [CrossRef]
81. Pan, H.; Li, X.; Qiao, B. New Insights to Understand the Influence of Nb/Mo on Hydrogen Embrittlement Resistance of Warm-Rolled Medium-Mn Steels. *J. Mater. Eng. Perform.* **2022**, *31*, 3228–3233. [CrossRef]
82. Jo, M.C.; Yoo, J.; Kim, S.; Kim, S.; Oh, J.; Bian, J.; Sohn, S.S.; Lee, S. Effects of Nb and Mo alloying on resistance to hydrogen embrittlement in 1.9 GPa-grade hot-stamping steels. *Mater. Sci. Eng. A* **2020**, *789*, 139656. [CrossRef]
83. Okuno, K.; Takai, K. Extraction of reversible hydrogen trapped on prior austenite grain boundaries and promoting intergranular fracture in the elastic region of tempered martensitic steel by utilizing frozen-in hydrogen distribution at −196 °C. *Acta Mater.* **2023**, *259*, 119291. [CrossRef]
84. Shi, R.J.; Chen, L.; Wang, Z.D.; Yang, X.S.; Qiao, L.J.; Pang, X.L. Quantitative investigation on deep hydrogen trapping in tempered martensitic steel. *J. Alloys Compd.* **2021**, *854*, 157218. [CrossRef]
85. Chen, W.J.; Wei, Z.Y.; Zhang, S.H.; Ge, M.K.; Dai, X.; Wu, S. Microstructure evolution and hydrogen embrittlement mechanism of a 2200 MPa press-hardened steel with tempering treatment. *Mater. Charact.* **2025**, *223*, 114955. [CrossRef]
86. Sun, H.L.; Lv, W.T.; Yang, Y.; Li, D.D.; Yan, L.H.; Pang, X.L.; He, Y.; Gao, K.W. Optimizing the hydrogen embrittlement resistance by tuning the structures of Cu-rich nanoprecipitates in high strength martensite stainless steels. *Acta Mater.* **2023**, *246*, 118722. [CrossRef]

87. Zhou, C.S.; Jiang, C.C.; Jin, Y.; Zhou, H.B.; Qiu, Q.X.; Hu, Y.Q.; Xie, Y.C.; Zhang, L.; Zheng, J.Y. The regulation of dislocation and precipitated phase improving hydrogen embrittlement resistance of pipeline steel in high pressure hydrogen environment. *Int. J. Fatigue* **2025**, *190*, 108657. [CrossRef]
88. Li, X.F.; Zhang, J.; Cui, Y.; Djukic, M.B.; Feng, H.; Wang, Y.F. Review of the hydrogen embrittlement and interactions between hydrogen and microstructural interfaces in metallic alloys: Grain boundary, twin boundary, and nano-precipitate. *Int. J. Hydrogen Energy* **2024**, *72*, 74–109. [CrossRef]
89. Huang, F.; Li, X.G.; Liu, J.; Qu, Y.M.; Du, C.W. Effects of alloying elements, microstructure, and inclusions on hydrogen induced cracking of X120 pipeline steel in wet H_2S sour environment. *Mater. Corros.* **2012**, *63*, 59. [CrossRef]
90. Entezari, E.; Velázquez, J.L.G.; López, D.R.; Zúñiga, M.A.B.; Mousavi, H.; Davani, R.K.Z.; Szpunar, J. An experimental and statistical study on the characteristics of non-metallic inclusions that serve as hydrogen-induced crack nucleation sites in pipeline steel. *Eng. Fail. Anal.* **2023**, *154*, 107695. [CrossRef]
91. Beidokhti, B.; He, P.; Kokabi, A.H.; Dolati, A. Control of hydrogen cracking in the welded steel using microstructural traps. *Mater. Sci. Technol.* **2017**, *33*, 408. [CrossRef]
92. Chen, Y.; Liu, J.; Huang, F. Influence of inclusions on hydrogen-induced delayed cracking in hot stamping steels. *J. Iron Steel Res. Int.* **2019**, *26*, 1199–1208. [CrossRef]
93. Peng, Z.X.; Liu, J.; Huang, F.; Hu, Q.; Cheng, Z.Y.; Liu, S.; Cheng, Y.F. Effect of submicron-scale MnS inclusions on hydrogen trapping and HlC susceptibility of X70 pipeline steels. *Steel Res. Int.* **2018**, *89*, 1700566. [CrossRef]
94. Liou, H.; Shieh, R.I.; Wei, F.; Wang, S. Roles of microalloying elements in hydrogen induced cracking resistant property of HSLA steels. *Corrosion* **1993**, *49*, 389. [CrossRef]
95. Li, L.F.; Song, B.; Cheng, J.; Yang, Z.B.; Cai, Z.Y. Effects of vanadium precipitates on hydrogen trapping efficiency and hydrogen induced cracking resistance in X80 pipeline steel. *Int. J. Hydrogen Energy* **2018**, *43*, 17353. [CrossRef]
96. Jin, T.Y.; Liu, Z.Y.; Cheng, Y.F. Effect of non-metallic inclusions on hydrogen-induced cracking of API5L, X100 steel. *Int. J. Hydrogen Energy* **2010**, *35*, 8014. [CrossRef]
97. Song, K.K.; Cao, S.; Bao, Y.; Qian, P.; Su, Y.J. Designing hydrogen embrittlement-resistant grain boundary in steel by alloying elements segregation: First-principles calculations. *Appl. Surf. Sci.* **2024**, *656*, 159684. [CrossRef]
98. Sun, B.; Lu, W.; Gault, B. Chemical heterogeneity enhances hydrogen resistance in high-strength steels. *Nat. Mater.* **2021**, *20*, 1629–1634. [CrossRef]
99. Mao, L.Y.; Luo, Z.A.; Huang, C.; Wang, Y.Q.; Duan, R.H.; Zhang, X.M. Effects of grain boundary character distribution on hydrogen-induced cracks initiation and propagation at different strain rates in a nickel-saving and high-nitrogen austenitic stainless steel. *Mater. Sci. Eng. A* **2023**, *826*, 144509. [CrossRef]
100. Kwon, Y.J.; Jung, S.P.; Lee, B.J.; Lee, C.S. Grain boundary engineering approach to improve hydrogen embrittlement resistance in FeMnC TWIP steel. *Int. J. Hydrogen Energy* **2018**, *43*, 10129–10140. [CrossRef]
101. Kwon, Y.J.; Seo, H.J.; Kim, J.N.; Lee, C.S. Effect of grain boundary engineering on hydrogen embrittlement in Fe-Mn-C TWIP steel at various strain rates. *Corros. Sci.* **2018**, *142*, 213–221. [CrossRef]
102. Xi, X.H.; Liu, Z.K.; Qin, Z.B.; Wu, T.; Wang, J.L.; Xu, N.; Chen, L.Q. Enhancement of the resistance to hydrogen embrittlement by tailoring grain boundary characteristics in a low carbon high strength steel. *J. Mater. Res. Technol.* **2023**, *27*, 7119–7127. [CrossRef]
103. Lu, T.; Niu, G.J.; Xu, Y.P.; Wang, J.; An, Z.Q.; Liu, H.D.; Zhou, H.S.; Ding, F.; Luo, G.N.; Li, X.C. Molecular dynamics study of the diffusion properties of H in Fe with point defects. *Fusion Eng. Des.* **2016**, *113*, 340–345. [CrossRef]
104. Díaz, A.; Alegre, J.M.; Cuesta, I.I.; Pañeda, E.M. A COMSOL framework for predicting hydrogen embrittlement, Part II: Phase field fracture. *Eng. Fract. Mech.* **2025**, *319*, 111008. [CrossRef]
105. Cheng, Y.J.; Yang, C.F.; Xue, G.; Wang, T.; Zhang, L.; Li, M.E. Investigation of interaction between α-Fe metal and H atom by ab-initio method. *Acta Phys. Sin.* **2020**, *69*, 053101. [CrossRef]
106. He, Y.; Li, Y.J.; Chen, C.F.; Yu, H.B. Diffusion coefficient of hydrogen interstitial atom in α-Fe, γ-Fe and ε-Fe crystals by first-principle calculations. *Int. J. Hydrogen Energy* **2017**, *42*, 27438–27445. [CrossRef]
107. Jemblie, L.; Olden, V.; Mainçon, P.; Akselsen, O.M. Cohesive zone modelling of hydrogen induced cracking on the interface of clad steel pipes. *Int. J. Hydrogen Energy* **2017**, *42*, 28622–28634. [CrossRef]
108. Toribio, J.; Kharin, V.; Vergara, D.; Blanco, J.A.; Ballesteros, J.G. Influence of residual stresses and strains generated by cold drawing on hydrogen embrittlement of prestressing steels. *Corros. Sci.* **2007**, *49*, 3557–3569. [CrossRef]
109. An, T.; Peng, H.T.; Bai, P.P.; Zheng, S.Q.; Wen, X.L.; Zhang, L. Influence of hydrogen pressure on fatigue properties of X80 pipeline steel. *Int. J. Hydrogen Energy* **2017**, *42*, 15669–15678. [CrossRef]
110. Yin, H.; Cui, D.C.; Xiong, L.; Yu, B.T.; Wei, B.X.; Fan, J.J.; Dong, L.J.; Xu, J.; Yu, C.K.; Sun, C. Hydrogen embrittlement susceptibility of X65 pipeline steel pre-charged with hydrogen in hydrogen-blended natural gas with CO_2: Influences of pressure and strain rate. *Corros. Commun.* 2026, *in press*.
111. Li, H.Y.; Niu, R.M.; Li, W.; Lu, H.Z.; Cairney, J.; Chen, Y.S. Hydrogen in pipeline steels: Recent advances in characterization and embrittlement mitigation. *J. Nat. Gas Sci. Eng.* **2022**, *105*, 104709. [CrossRef]

112. Tsiklios, C.; Hermesmann, M.; Müller, T.E. Hydrogen transport in large-scale transmission pipeline networks: Thermodynamic and environmental assessment of repurposed and new pipeline configurations. *Appl. Energy* **2022**, *327*, 120097. [CrossRef]
113. Xing, X.; Pang, Z.W.; Zhang, H.; Liu, J.G.; Cui, G. Study of temperature effect on hydrogen embrittlement in X70 pipeline steel. *Corros. Sci.* **2024**, *230*, 111939. [CrossRef]
114. Li, J.Q.; Wu, Z.Y.; Zhu, L.J.; Zhang, Z.W.; Teng, L.; Zhang, L.; Lu, C.; Wang, R.; Zhang, C. Investigations of temperature effects on hydrogen diffusion and hydrogen embrittlement of X80 pipeline steel under electrochemical hydrogen charging environment. *Corros. Sci.* **2023**, *223*, 111460. [CrossRef]
115. Liu, C.W.; Pei, Y.B.; Cui, Z.X.; Li, X.J.; Yang, H.C.; Xing, X.; Duan, P.F.; Li, L.L.; Li, Y.X. Study on the stratification of the blended gas in the pipeline with hydrogen into natural gas. *Int. J. Hydrogen Energy* **2023**, *48*, 5186–5196. [CrossRef]
116. Wang, Y.F.; Li, Y.Z.; Huang, Y.T.; Xie, H.L.; Wu, W.J. Effect of grain size on hydrogen embrittlement of 304L, austenitic stainless steel. *J. Chin. Soc. Corros. Prot.* **2023**, *43*, 494–506. [CrossRef]
117. Liu, L.G.; Xiao, H.; Li, Q.; Liu, Y.; Li, P.S.; Yang, Z.Q.; Yu, H. Evaluation of the fracture toughness of X70 pipeline steel with ferrite-bainite microstructure. *Mater. Sci. Eng. A* **2017**, *688*, 388–395. [CrossRef]
118. Zhang, Y.C.; Jiang, W.C.; Tu, S.T.; Zhang, X.C. Fracture toughness assessment of the X80 steel by nanoindentation technique and a modified constitutive model. *Theor. Appl. Fract. Mech.* **2022**, *117*, 103195. [CrossRef]
119. Han, Y.D.; Wang, R.Z.; Wang, H.; Xu, L.Y. Hydrogen embrittlement sensitivity of X100 pipeline steel under different pre-strain. *Int. J. Hydrogen Energy* **2019**, *44*, 22380–22393. [CrossRef]
120. Hejazi, D.; Haq, A.J.; Yazdipour, N.; Dunne, D.P.; Calka, A.; Barbaro, F.; Pereloma, E.V. Effect of manganese content and microstructure on the susceptibility of X70 pipeline steel to hydrogen cracking. *Mater. Sci. Eng. A* **2012**, *551*, 40–49. [CrossRef]
121. Gyaabeng, M.; Ahmed, R.; Rhythm, S.; Ahmed, N.; Teodoriu, C. Impacts of gas composition and temperature on the hydrogen embrittlement of pipeline steels. *Eng. Fail. Anal.* **2025**, *181*, 109964. [CrossRef]
122. Doshida, T.; Takai, K. Dependence of hydrogen-induced lattice defects and hydrogen embrittlement of cold-drawn pearlitic steels on hydrogen trap state, temperature, strain rate and hydrogen content. *Acta Mater.* **2014**, *79*, 93–107. [CrossRef]
123. Xing, X.; Cheng, R.; Cui, G.; Liu, J.G.; Gou, J.X.; Yang, C.; Li, Z.L.; Yang, F. Quantification of the temperature threshold of hydrogen embrittlement in X90 pipeline steel. *Mater. Sci. Eng. A* **2021**, *800*, 140118. [CrossRef]
124. Momotani, Y.; Shibata, A.; Tsuji, N. Hydrogen embrittlement behaviors at different deformation temperatures in as-quenched low-carbon martensitic steel. *Int. J. Hydrogen Energy* **2022**, *47*, 3131–3140. [CrossRef]
125. Galliano, F.; Andrieu, E.; Blanc, C.; Cloue, J.M.; Connetable, D.; Odemer, G. Effect of trapping and temperature on the hydrogen embrittlement susceptibility of alloy 718. *Mater. Sci. Eng. A* **2014**, *611*, 370–382. [CrossRef]
126. Zhang, T.M.; Zhao, W.M.; Zhao, Y.J.; Ouyang, K.; Deng, Q.S.; Wang, Y.L.; Jiang, W. Effects of surface oxide films on hydrogen permeation and susceptibility to embrittlement of X80 steel under hydrogen atmosphere. *Int. J. Hydrogen Energy* **2018**, *43*, 3353–3365. [CrossRef]
127. Ilin, D.N.; Saintier, N.; Olive, J.M.; Abgrall, R.; Aubert, I. Simulation of hydrogen diffusion affected by stress-strain heterogeneity in polycrystalline stainless steel. *Int. J. Hydrogen Energy* **2014**, *39*, 2418–2422. [CrossRef]
128. Barrera, O.; Bombac, D.; Chen, Y. Understanding and mitigating hydrogen embrittlement of steels: A review of experimental, modelling and design progress from atomistic to continuum. *J. Mater. Sci.* **2018**, *53*, 6251–6290. Correction in *J. Mater. Sci.* **2018**, *53*, 10593–10594. [CrossRef]
129. Okayasu, M.; Motojima, J. Microstructure-dependent hydrogen diffusion and trapping in high-tensile steel. *Mater. Sci. Eng. A* **2020**, *790*, 139418. [CrossRef]
130. Amaro, R.L.; Rustagi, N.; Findley, K.O.; Drexler, E.S.; Slifka, A.J. Modeling the fatigue crack growth of X100 pipeline steel in gaseous hydrogen. *Int. J. Fatigue* **2014**, *59*, 262–271. [CrossRef]
131. Huang, L.; Chen, D.; Xie, D. Quantitative tests revealing hydrogen-enhanced dislocation motion in α-iron. *Nat. Mater.* **2023**, *22*, 710–716. [CrossRef] [PubMed]
132. Behvar, A.; Haghshenas, M.; Djukic, M.B. Hydrogen embrittlement and hydrogen-induced crack initiation in additively manufactured metals: A critical review on mechanical and cyclic loading. *Int. J. Hydrogen Energy* **2024**, *8*, 1214–1239. [CrossRef]
133. Fu, Z.H.; Li, T.; Shan, M.L.; Gou, G.Q.; Zhu, Z.Y.; Ma, C.P.; Gao, W.; Hu, Y.C. Hydrogen atoms on the SCC behavior of SUS301L-MT stainless steel laser-arc hybrid welded joints. *Corros. Sci.* **2019**, *148*, 272–280. [CrossRef]
134. Xu, T.L.; Guo, S.H.; Fu, B.W.; Ma, X.L.; Han, H.Y.; Li, Y.L.; Jiang, H.Y. Hydrogen diffusion simulation of the X80 pipeline steel girth weld zone considering the synergistic effect of the structure-stress-concentration field. *Eng. Fail. Anal.* **2021**, *160*, 108205. [CrossRef]
135. Qu, L.; Wei, B.X.; Dong, L.J.; Yu, C.K.; Xu, J.; Sun, C. Hydrogen embrittlement of X80 pipeline steel under cathodic and gaseous hydrogen exposure in simulated pipeline environments. *Int. J. Hydrogen Energy* **2026**, *197*, 152603. [CrossRef]
136. Amaro, R.L.; Drexler, E.S.; Slifka, A.J. Fatigue crack growth modeling of pipeline steels in high pressure gaseous hydrogen. *Int. J. Fatigue* **2014**, *62*, 249–257. [CrossRef]

137. Stalheim, D.; Boggess, T.; Marchi, C.S.; Jansto, S.; Somerday, B.; Muralidharan, G.; Sofronis, P. Microstructure and Mechanical Property Performance of Commercial Grade API Pipeline Steels in High Pressure Gaseous Hydrogen. In Proceedings of the 2010 8th International Pipeline Conference, Calgary, AB, Canada, 27 September–1 October 2010; ASME: New York, NY, USA, 2011; Volume 2, pp. 529–537. [CrossRef]
138. Marchi, S.; Somerday, C.; Nibur, B.P.; Stalheim, K.A.; Boggess, T.D.G.; Jansto, S. Fracture and Fatigue of Commercial Grade API Pipeline Steels in Gaseous Hydrogen. In Proceedings of the ASME 2010 Pressure Vessels and Piping Division/K-PVP Conference, Bellevue, WA, USA, 18–22 July 2010; ASME: New York, NY, USA, 2011; Volume 6, pp. 939–948. [CrossRef]
139. Marchi, S.; Somerday, C.; Nibur, B.P.; Stalheim, K.A.; Boggess, T.D.G.; Jansto, S. Fracture Resistance and Fatigue Crack Growth of X80 Pipeline Steel in Gaseous Hydrogen. In Proceedings of the ASME 2011 Pressure Vessels and Piping Conference, Baltimore, MD, USA, 17–21 July 2011; ASME: New York, NY, USA, 2012; Volume 6, pp. 841–849. [CrossRef]
140. Slifka, A.J.; Drexler, E.S.; Nanninga, N.E.; Levy, Y.S.; McColskey, J.D.; Amaro, R.L.; Stevenson, A.E. Fatigue crack growth of two pipeline steels in a pressurized hydrogen environment. *Corros. Sci.* **2014**, *78*, 313–321. [CrossRef]
141. Nguyen, T.T.; Park, J.S.; Kim, W.S.; Nahm, S.H.; Beak, U.B. Environment hydrogen embrittlement of pipeline steel X70 under various gas mixture conditions with in situ small punch tests. *Mater. Sci. Eng. A* **2020**, *781*, 139114. [CrossRef]
142. Zhang, H.W.; Zhao, J.; Li, J.F.; Yu, B.; Wang, J.L.; Lyu, R.; Xi, Q. Research progress on corrosion and hydrogen embrittlement in hydrogen-natural gas pipeline transportation. *Nat. Gas Ind. B* **2023**, *10*, 570–582. [CrossRef]
143. Mustapha, A.; Charles, E.A.; Hardie, D. Evaluation of environment-assisted cracking susceptibility of a grade X100 pipeline steel. *Corros. Sci.* **2012**, *54*, 5–9. [CrossRef]
144. Nanninga, N.E.; Levy, Y.S.; Drexler, E.S.; Condon, R.T.; Stevenson, A.E.; Slifka, A.J. Comparison of hydrogen embrittlement in three pipeline steels in high pressure gaseous hydrogen environments. *Corros. Sci.* **2012**, *59*, 1–9. [CrossRef]
145. Li, Y.X.; Zhang, R.; Liu, C.W.; Wang, C.L. Hydrogen embrittlement behavior of typical hydrogen-blended natural gas pipeline steel. *Oil Gas Storage Transp.* **2022**, *41*, 732–742.
146. Ran, L.L.; Chen, S.; Li, B.; Zhang, Z.H.; Zhang, K.H.; Wang, B.; Liu, Q.Y.; Jia, S.J. Improvement of hydrogen embrittlement resistance of X52 pipeline steel by Nb-V composite microalloying design: Hydrogen trap regulation and mechanism. *Int. J. Hydrogen Energy* **2025**, *192*, 152343. [CrossRef]
147. Nguyen, T.T.; Bae, K.O.; Jaeyeong, P.; Nahm, S.H.; Baek, U.B. Damage associated with interactions between microstructural characteristics and hydrogen/methane gas mixtures of pipeline steels. *Int. J. Hydrogen Energy* **2022**, *47*, 31499–31520. [CrossRef]
148. Briottet, L.; Batisse, R.; Dinechin, G.; Langlois, P.; Thiers, L. Recommendations on X80 steel for the design of hydrogen gas transmission pipelines. *Int. J. Hydrogen Energy* **2012**, *37*, 9423–9430. [CrossRef]
149. Laureys, A.; Depraetere, R.; Cauwels, M.; Depover, T.; Hertelé, S.; Verbeken, K. Use of existing steel pipeline infrastructure for gaseous hydrogen storage and transport: A review of factors affecting hydrogen induced degradation. *J. Nat. Gas Sci. Eng.* **2022**, *101*, 104534. [CrossRef]
150. Guan, H.P.; Lin, Z.X.; Li, Y.X.; Liu, Q.; Xing, Y.Y.; Wang, J.; Wang, X.Y. Hydrogen embrittlement susceptibility of the X70 pipeline steel substrate and weld in simulated coal gas containing hydrogen environment. *Chin. J. Eng.* **2017**, *39*, 535–541. [CrossRef]
151. Lang, F.; Huang, F.; Yue, J. Hydrogen trapping and hydrogen embrittlement (HE) susceptibility of X70 grade high-strength, acid-resistant, submarine pipeline steel with Mg treatment. *J. Mater. Res. Technol.* **2023**, *24*, 16. [CrossRef]
152. Alvaro, A.; Olden, V.; Macadre, A.; Akselsen, O.M. Hydrogen embrittlement susceptibility of a weld simulated X70 heat affected zone under H2 pressure. *Mater. Sci. Eng. A* **2014**, *597*, 29–36. [CrossRef]
153. Shang, J.; Zheng, J.Y.; Hua, Z.L.; Li, Y.H.; Gu, C.H.; Cui, T.C.; Meng, B. Effects of stress concentration on the mechanical properties of X70 in high-pressure hydrogen-containing gas mixtures. *Int. J. Hydrogen Energy* **2020**, *45*, 28204–28215. [CrossRef]
154. Wang, C.L.; Zhang, J.X.; Liu, C.W.; Hu, Q.H.; Zhang, R.; Xu, X.S.; Yang, H.C.; Ning, Y.X.; Li, Y.X. Study on hydrogen embrittlement susceptibility of X80 steel through in-situ gaseous hydrogen permeation and slow strain rate tensile tests. *Int. J. Hydrogen Energy* **2023**, *48*, 243–256. [CrossRef]
155. Zhou, D.J.; Li, T.T.; Huang, D.W.; Wu, Y.; Huang, Z.S.; Xiao, W.; Wang, Q.; Wang, X.Y. The experiment study to assess the impact of hydrogen blended natural gas on the tensile properties and damage mechanism of X80 pipeline steel. *Int. J. Hydrogen Energy* **2021**, *46*, 7402–7414. [CrossRef]
156. Wu, X.; Teng, M.J.; Jia, W.L.; Cai, J.J. Study on the mechanical properties of X80 pipeline steel under pre-charged high-pressure gaseous hydrogen. *Int. J. Hydrogen Energy* **2024**, *84*, 39–52. [CrossRef]
157. Moro, I.; Briottet, L.; Lemoine, P.; Andrieu, E.; Blanc, C.; Odemer, G. Hydrogen embrittlement susceptibility of a high strength steel X80. *Mater. Sci. Eng. A* **2010**, *527*, 7252–7260. [CrossRef]
158. Myhre, A.O.; Wan, D.; Sendrowicz, A.; Olden, V.; Matsunaga, H.; Alvaro, A.; Vinogradov, A. Hydrogen enhanced fatigue crack growth rates in a vintage and a modern X65 pipeline steel. *Int. J. Fatigue* **2025**, *201*, 109186. [CrossRef]
159. Takakuwa, O.; Ogawa, Y.; Okazaki, S.; Nakamura, M.; Matsunaga, H. A mechanism behind hydrogen-assisted fatigue crack growth in ferrite-pearlite steel focusing on its behavior in gaseous environment at elevated temperature. *Corros. Sci.* **2020**, *168*, 108558. [CrossRef]

160. Shi, H.; Xing, Y.Y.; Wang, X.Y.; Wang, J. Applicability Evaluation Method of Coal Synthetic Natural Gas Pipeline Material. *Corros. Prot.* **2019**, *40*, 48–51, 65.
161. Ronevich, J.A.; Somerday, B.P.; Feng, Z. Hydrogen accelerated fatigue crack growth of friction stir welded X52 steel pipe. *Int. J. Hydrogen Energy* **2017**, *42*, 4259–4268. [CrossRef]
162. Drexler, E.S.; Slifka, A.J.; Amaro, R.L.; Sowards, J.W.; Connolly, M.; Martin, M.L.; Lauria, D.S. Fatigue testing of pipeline welds and heat-affected zones in pressurized hydrogen gas. *J. Res. Natl. Inst. Stand. Technol.* **2019**, *124*, 124008. [CrossRef]
163. Shi, X.B.; Yan, W.; Wang, W. HIC and SSC Behavior of High-Strength Pipeline Steels. *Acta Metall. Sin. (Engl. Lett.)* **2015**, *28*, 799–808. [CrossRef]
164. Malede, Y.C.; Adesina, A.Y.; Ashraf, F.; Sorour, A.A. Hydrogen-induced damage of materials: A review of testing and evaluation methods, and hydrogen mapping techniques. *Renew. Sustain. Energy Rev.* **2025**, *215*, 115528. [CrossRef]
165. Jack, T.A.; Pourazizi, R.; Ohaeri, E.; Szpunar, J.; Zhang, J.M.; Qu, J.B. Investigation of the hydrogen induced cracking behaviour of API 5L X65 pipeline steel. *Int. J. Hydrogen Energy* **2020**, *45*, 17671–17684. [CrossRef]
166. Thomas, A.; Szpunar, J.A. Hydrogen diffusion and trapping in X70 pipeline steel. *Int. J. Hydrogen Energy* **2020**, *45*, 2390–2404. [CrossRef]
167. Liu, W.Q.; Liu, Q.D.; Gu, J.F. Development and application of atom probe tomography. *Acta Metall. Sin.* **2013**, *49*, 1025–1031. [CrossRef]
168. Chen, Y.S.; Haley, D.; Gerstl, S.S.A.; London, A.J.; Sweeney, F.; Wepf, R.A.; Rainforth, W.M.; Bagot, P.A.J.; Moody, M.P. Direct observation of individual hydrogen atoms at trapping sites in a ferritic steel. *Science* **2017**, *355*, 1196. [CrossRef]
169. Takahashi, J.; Kawakami, K.; Kobayashi, Y.; Tarui, T. The first direct observation of hydrogen trapping sites in TiC precipitation-hardening steel through atom probe tomography. *Scr. Mater.* **2010**, *63*, 261–264. [CrossRef]
170. Zhang, B.; Zhu, Q.; Xu, C.; Li, C.; Ma, Y.; Ma, Z.; Liu, S.; Shao, R.; Xu, Y.; Jiang, B.; et al. Atomic-scale insights on hydrogen trapping and exclusion at incoherent interfaces of nanoprecipitates in martensitic steels. *Nat. Commun.* **2022**, *13*, 3858. [CrossRef]
171. Zhou, X.Y.; Zhu, J.H.; Wu, Y.; Yang, X.S.; Lookman, T.; Wu, H.H. Machine learning assisted design of FeCoNiCrMn high-entropy alloys with ultra-low hydrogen diffusion coefficients. *Acta Mater.* **2022**, *224*, 117535. [CrossRef]
172. Kwon, H.; Shiga, M.; Kimizuka, H.; Oda, T. Accurate description of hydrogen diffusivity in bcc metals using machine-learning moment tensor potentials and path-integral methods. *Acta Mater.* **2023**, *247*, 118739. [CrossRef]
173. Al-Hawary, S.I.S.; Sari, A.; Askar, S.; Pallathadka, H.; Asaad, R.R.; Sharma, M.K. Guided analysis of fracture toughness and hydrogen-induced embrittlement crack growth rate in quenched-and-tempered steels using machine learning. *Int. J. Press. Vessel. Pip.* **2024**, *210*, 105247. [CrossRef]
174. Kim, S.G.; Shin, S.H.; Hwang, B. Machine learning approach for prediction of hydrogen environment embrittlement in austenitic steels. *J. Mater. Res. Technol.* **2022**, *19*, 2794–2798. [CrossRef]
175. Zhang, Y.J.; Ai, Y.B.; Zhang, W.D. Physics informed ensemble learning used for interval prediction of fracture toughness of pipeline steels in hydrogen environments. *Theor. Appl. Fract. Mech.* **2024**, *130*, 104302. [CrossRef]
176. Shi, R.J.; Ma, Y.; Wang, Z.D.; Gao, L.; Yang, X.S.; Qiao, L.J.; Pang, X.L. Atomic-scale investigation of deep hydrogen trapping in NbC/α-Fe semi-coherent interfaces. *Acta Mater.* **2020**, *200*, 686–698. [CrossRef]
177. Cheng, G.; Wang, X.L.; Chen, K.Y.; Zhang, Y.; Venkatesh, T.A.; Wang, X.L.; Li, Z.Z.; Yang, J. Probing the effects of hydrogen on the materials used for large-scale transport of hydrogen through multi-scale simulations. *Renew. Sustain. Energy Rev.* **2023**, *182*, 113353. [CrossRef]
178. Gong, P.; Turk, A.; Nutter, J.; Yu, F.; Wynne, B.; Rivera-Diaz-del-Castillo, P.; Rainforth, W.M. Hydrogen embrittlement mechanisms in advanced high strength steel. *Acta Mater.* **2022**, *223*, 117488. [CrossRef]
179. Ohaeri, E.; Szpunar, J.; Fazeli, F.; Arafin, M. Hydrogen induced cracking susceptibility of API 5L X70 pipeline steel in relation to microstructure and crystallographic texture developed after different thermomechanical treatments. *Mater. Charact.* **2018**, *145*, 142–156. [CrossRef]
180. Ohaeri, E.; Omale, J.; Rahman, K.M.M.; Szpunar, J. Effect of post-processing annealing treatments on microstructure development and hydrogen embrittlement in API 5L X70 pipeline steel. *Mater. Charact.* **2020**, *161*, 110124. [CrossRef]
181. Park, G.T.; Koh, S.U.; Jung, H.G.; Kim, K.Y. Effect of microstructure on the hydrogen trapping efficiency and hydrogen induced cracking of linepipe steel. *Corros. Sci.* **2008**, *50*, 1865–1871. [CrossRef]
182. Liu, J.G.; Guo, Y.G.; Xing, X.; Zhang, X.W.; Yang, Y.P.; Cui, G. A comprehensive review on hydrogen permeation barrier in the hydrogen transportation pipeline: Mechanism, application, preparation, and recent advances. *Int. J. Hydrogen Energy* **2025**, *101*, 504–528. [CrossRef]
183. Shang, J.; Chen, W.F.; Zheng, J.Y.; Hua, Z.L.; Zhang, L.; Zhou, C.S.; Gu, C.H. Enhanced hydrogen embrittlement of low-carbon steel to natural gas/hydrogen mixtures. *Scr. Mater.* **2020**, *189*, 67–71. [CrossRef]
184. Meng, B.; Gu, C.H.; Zhang, L.; Zhou, C.S.; Li, X.Y.; Zhao, Y.Z.; Zheng, J.Y.; Chen, X.Y.; Han, Y. Hydrogen effects on X80 pipeline steel in high-pressure natural gas/hydrogen mixtures. *Int. J. Hydrogen Energy* **2017**, *42*, 7404–7412. [CrossRef]

185. Michler, T.; Boitsov, I.E.; Malkov, I.L.; Yukhimchuk, A.A.; Naumann, J. Assessing the effect of low oxygen concentrations in gaseous hydrogen embrittlement of DIN 1.4301 and 1.1200 steels at high gas pressures. *Corros. Sci.* **2012**, *65*, 169–177. [CrossRef]
186. Somerday, B.P.; Sofronis, P.; Nibur, K.A.; Marchi, C.S.; Kirchheim, R. Elucidating the variables affecting accelerated fatigue crack growth of steels in hydrogen gas with low oxygen concentrations. *Acta Mater.* **2013**, *61*, 6153–6170. [CrossRef]
187. Shi, K.; Xiao, S.; Ruan, Q.D.; Wu, H.; Chen, G.H.; Zhou, C.L.; Jiang, S.H.; Xi, K.; He, M.H.; Chu, P.K. Hydrogen permeation behavior and mechanism of multi-layered graphene coatings and mitigation of hydrogen embrittlement of pipe steel. *Appl. Surf. Sci.* **2022**, *573*, 151529. [CrossRef]
188. An, T.; Li, S.J.; Qu, J.L.; Shi, J.; Zhang, S.; Chen, L.Q.; Zheng, S.Q.; Yang, F. Effects of shot peening on tensile properties and fatigue behavior of X80 pipeline steel in hydrogen environment. *Int. J. Fatigue* **2019**, *129*, 105235. [CrossRef]
189. Levchuk, D.; Koch, F.; Maier, H.; Bolt, H. Deuterium permeation through Eurofer and α-alumina coated Eurofer. *J. Nucl. Mater.* **2004**, *328*, 103–106. [CrossRef]
190. Forcey, K.S.; Ross, D.K.; Wu, C.H. The formation of hydrogen permeation barriers on steels by aluminizing. *J. Nucl. Mater.* **1991**, *182*, 36–51. [CrossRef]
191. Wang, J.P.; Lu, Z.X.; Ling, Y.H.; Wang, R.G.; Li, Y.H.; Zhou, Q.Y.; Zhang, Z.J. Hydrogen permeation properties of Cr_xC_y@Cr_2O_3/Al_2O_3 composite coating derived from selective oxidation of a CrC alloy and atomic layer deposition. *Int. J. Hydrogen Energy* **2018**, *43*, 21133–21141. [CrossRef]
192. Zhou, Q.Y.; Ling, Y.H.; Lu, Z.X.; Luo, Y.; Wang, J.P.; Zhang, Z.J. Characteristics of hydrogen plasma treatment on $Al_2O_3/Cr_xO_y/Al_mO_n$ composite film via Al-ion-implantation and ultra-low partial pressure oxidation. *Surf. Coat. Technol.* **2020**, *395*, 125917. [CrossRef]
193. Izawa, C.; Wagner, S.; Deutges, M.; Martín, M.; Weber, S.; Pargeter, R.; Michler, T.; Uchida, H.H.; Gemma, R.; Pundt, A. Role of surface oxide layers in the hydrogen embrittlement of austenitic stainless steels: A TOF-SIMS study. *Acta Mater.* **2019**, *180*, 329–340. [CrossRef]
194. Nam, T.H.; Lee, J.H.; Choi, S.R.; Yoo, J.B.; Kim, J.G. Graphene coating as a protective barrier against hydrogen embrittlement. *Int. J. Hydrogen Energy* **2014**, *39*, 11810–11817. [CrossRef]
195. Kim, Y.S.; Kim, J.G. Electroplating of reduced-graphene oxide on austenitic stainless steel to prevent hydrogen embrittlement. *Int. J. Hydrogen Energy* **2017**, *42*, 27428–27437. [CrossRef]
196. Chatzidouros, E.V.; Papazoglou, V.J.; Tsiourva, T.E.; Pantelis, D.I. Hydrogen effect on fracture toughness of pipeline steel welds, with in situ hydrogen charging. *Int. J. Hydrogen Energy* **2011**, *36*, 12626–12643. [CrossRef]
197. Wei, H.T.; Duan, B.Q.; Shi, X.S.; Gao, R.Z.; Hua, Z.L.; Qiu, S.Y.; Zhao, Y.M. Influence of hydrogen in natural gas mixed hydrogen environment on mechanical properties of X80 pipeline steel. *Int. J. Hydrogen Energy* **2024**, *54*, 908–921. [CrossRef]
198. Zhang, S.; An, T.; Zheng, S.Q.; Li, J.; Li, S.J.; Chen, L.Q. The effects of double notches on the mechanical properties of a high-strength pipeline steel under hydrogen atmosphere. *Int. J. Hydrogen Energy* **2020**, *45*, 23134–23141. [CrossRef]
199. Zhou, C.S.; Ye, B.G.; Song, Y.Y.; Cui, T.C.; Xu, P.; Zhang, L. Effects of internal hydrogen and surface-absorbed hydrogen on the hydrogen embrittlement of X80 pipeline steel. *Int. J. Hydrogen Energy* **2019**, *44*, 22547–22558. [CrossRef]
200. Jo, K.R.; Cho, L.; Sulistiyo, D.H.; Seo, E.J.; Kim, S.W.; Cooman, B.C.D. Effects of Al-Si coating and Zn coating on the hydrogen uptake and embrittlement of ultra-high strength press-hardened steel. *Surf. Coat. Technol.* **2019**, *374*, 1108–1119. [CrossRef]
201. Xu, X.S.; Zhang, R.; Wang, C.L.; Liu, C.W.; Zhang, J.; Li, Y.X. Experimental study on the temperature dependence of gaseous hydrogen permeation and hydrogen embrittlement susceptibility of X52 pipeline steel. *Eng. Fail. Anal.* **2024**, *155*, 107746. [CrossRef]